INTERIM REPORT

Full Scale Measurement and Modeling of the Acoustic Response of Proud and Buried Munitions at Frequencies from 1-30 kHz

SERDP Project MR-1665

AUGUST 2010

Steven G. Kargl
Kevin L. Williams
University of Washington

This document has been cleared for public release

SERDP
DOD ▪ EPA ▪ DOE

Report Documentation Page

Form Approved
OMB No. 0704-0188

Public reporting burden for the collection of information is estimated to average 1 hour per response, including the time for reviewing instructions, searching existing data sources, gathering and maintaining the data needed, and completing and reviewing the collection of information. Send comments regarding this burden estimate or any other aspect of this collection of information, including suggestions for reducing this burden, to Washington Headquarters Services, Directorate for Information Operations and Reports, 1215 Jefferson Davis Highway, Suite 1204, Arlington VA 22202-4302. Respondents should be aware that notwithstanding any other provision of law, no person shall be subject to a penalty for failing to comply with a collection of information if it does not display a currently valid OMB control number.

1. REPORT DATE **AUG 2010**	2. REPORT TYPE	3. DATES COVERED **00-00-2010 to 00-00-2010**
4. TITLE AND SUBTITLE **Full Scale Measurement and Modeling of the Acoustic Response of Proud and Buried Munitions at Frequencies from 1-30 kHz**		5a. CONTRACT NUMBER 5b. GRANT NUMBER 5c. PROGRAM ELEMENT NUMBER
6. AUTHOR(S)		5d. PROJECT NUMBER 5e. TASK NUMBER 5f. WORK UNIT NUMBER
7. PERFORMING ORGANIZATION NAME(S) AND ADDRESS(ES) **University of Washington,Applied Physics Laboratory,1013 NE 40th St,Seattle,WA,98105**		8. PERFORMING ORGANIZATION REPORT NUMBER
9. SPONSORING/MONITORING AGENCY NAME(S) AND ADDRESS(ES)		10. SPONSOR/MONITOR'S ACRONYM(S) 11. SPONSOR/MONITOR'S REPORT NUMBER(S)

12. DISTRIBUTION/AVAILABILITY STATEMENT
Approved for public release; distribution unlimited

13. SUPPLEMENTARY NOTES

14. ABSTRACT
A series of monostatic and bistatic acoustic scattering measurements were conducted to investigate discrimination and classi cation capabilities based on the acoustic response of targets for underwater un-exploded ordnance (UXO) applications. The measurements were performed during March 2010 and are referred to as Pond Experiment 2010 or simply PondEx10. The measurements utilized a rail system with a mobile tower and a stationary sonar tower. Each tower is instrumented with receivers while the sources are located only on the mobile tower. For PondEx10, eleven targets were deployed at two distinct horizontal ranges from the mobile tower system. Acoustic data were initially processed using synthetic aperture sonar (SAS) techniques, and the data were further processed to generate acoustic templates for the target strength as a function of frequency and aspect angle. Results of the processing of data collected from targets are presented. Also presented are the results associated with a processing technique that permits isolation of the response of an individual target, which is in close proximity to other targets.

15. SUBJECT TERMS

16. SECURITY CLASSIFICATION OF:			17. LIMITATION OF ABSTRACT	18. NUMBER OF PAGES	19a. NAME OF RESPONSIBLE PERSON
a. REPORT **unclassified**	b. ABSTRACT **unclassified**	c. THIS PAGE **unclassified**	**Same as Report (SAR)**	**62**	

This report was prepared under contract to the Department of Defense Strategic Environmental Research and Development Program (SERDP). The publication of this report does not indicate endorsement by the Department of Defense, nor should the contents be construed as reflecting the official policy or position of the Department of Defense. Reference herein to any specific commercial product, process, or service by trade name, trademark, manufacturer, or otherwise, does not necessarily constitute or imply its endorsement, recommendation, or favoring by the Department of Defense.

Second Interim Report for Project MR-1665
Full Scale Measurement and Modeling of the Acoustic Response of Proud and Buried Munitions at Frequencies from 1-30 kHz

POCS: Steven G. Kargl (PI) and Kevin L. Williams (co-PI)
Applied Physics Laboratory, University of Washington
1013 NE 40th St, Seattle WA 98105
kargl@apl.washington.edu, (206) 685–4677
williams@apl.washington.edu, (206) 543–3949

Abstract

A series of monostatic and bistatic acoustic scattering measurements were conducted to investigate discrimination and classification capabilities based on the acoustic response of targets for underwater unexploded ordnance (UXO) applications. The measurements were performed during March 2010 and are referred to as Pond Experiment 2010 or simply PondEx10. The measurements utilized a rail system with a mobile tower and a stationary sonar tower. Each tower is instrumented with receivers while the sources are located only on the mobile tower. For PondEx10, eleven targets were deployed at two distinct horizontal ranges from the mobile tower system. Acoustic data were initially processed using synthetic aperture sonar (SAS) techniques, and the data were further processed to generate acoustic templates for the target strength as a function of frequency and aspect angle. Results of the processing of data collected from targets are presented. Also presented are the results associated with a processing technique that permits isolation of the response of an individual target, which is in close proximity to other targets.

Introduction

Although the practice of disposing conventional and chemical munitions in coastal waters was discontinued during the 1970's, the environmental, economical, and even the recreational impact persists today [1]. In Overfield and Symons' overview of the Resources and UnderSea Threats (RUST) database [2], they note that over 2100 underwater sites are likely to contain munitions. Of those 2100 sites, verification has been completed on only slightly more than 50%. Schwartz and Brandenburg [3] summarize the current technologies available for underwater UXO applications. Their Table 1 includes metal detection (e.g., electromagnetic induction and magnetometers), chemical sensors (spectroscopy and fluorescence), and sonar. Metal detection and chemical sensors are typically restricted to short ranges; while the sonar technologies considered are limited in range (e.g., Didson system) or are limited by poor penetration into sediments (e.g., side-scan sonar) due to the high frequencies used. Furthermore, Schwartz and Brandenburg note that SAS is still a relatively new technology in UXO detection and that low-frequency SAS systems have demonstrated detection of proud and partially buried objects [4].

Low-frequency SAS systems with a wide bandwidth have several advantages over higher frequency sonar systems. Low frequencies offer greater detection ranges, which permits the rapid surveying of wider areas. In addition, low frequencies attain greater penetration depths into sediments, which permit detection of partially and completely buried munitions. The range resolution of a SAS system is related to the bandwidth of the transmitted signal where a wider bandwidth provides higher resolution. Thus, we report here on our preliminary analysis of UXO detection and discrimination by a low-frequency wide bandwidth SAS system. Our work compliments that of Bucaro *et al.* in that they consider isolated UXO in their research [4]. The experiments conducted during PondEx10 have multiple UXO in the field of view of the SAS system with a minimum separation distance of approximately 1.5 m.

Pond Experiment 2010

PondEx10 was carried out in a fresh water pond located at the Naval Surface Warfare Center, Panama City Division (NSWC PCD). This pond holds approximately 9 million gallons of water, and has nominal dimensions of 110 m in length and 80 m in width. The water depth at the location of the deployed target fields is $\sim$ 14 m. The bottom of the pond is covered with a $\sim$ 1.5 m thick layer of medium-fine sand. To

Figure 1: Underwater images of the several targets used during PondEx10.

prevent biological growth and fouling of the targets and equipment, the water is filtered and chlorinated. During the PondEx10 measurements, the sound speed in the water was found to be 1456 m/s. This sound speed estimate is based on the temperature readings from the divers' dive computers. A detailed drawing and aerial view of the pond can be found in [5].

Eleven targets were deployed in the measurements. The targets included a solid aluminum cylinder, an aluminum pipe, an inert 81 mm mortar (filled with cement), a solid steel artillery shell, two machined aluminum UXO, a machined steel UXO, a de-militarized 152 mm TP-T round, a de-militarized 155 mm empty howitzer projectile (without fuse or lifting eye), a small aluminum cylinder with a notch, and two rocks. As can be seen in Fig. 1, the sizes of the rocks are comparable to other targets. Figure 1 shows all of the targets except the solid aluminum cylinder. The machined aluminum and steel UXO were constructed from materials with known properties and are based on a CAD drawing of the solid steel artillery shell. The solid aluminum cylinder is 2 ft long with a 1 ft diameter; while the aluminum pipe is 2 ft long with an inner diameter of 1 ft and 3/8 inch wall thickness.

A rough layout of the 10 m target field is illustrated in Fig. 2. Divers first deployed the 21 m long rail system, which consists of three independent sections (see Fig. 1 in [5]). The sections are connected and leveled to establish a baseline for the geometry of the experiment. The divers then surveyed in two screw anchors at an 11 m horizontal range from the rail. The dashed lines in Fig. 2 depict temporary lines for siting the left screw anchor. A lightweight guide line is then stretched between the screw anchors and marked at 4, 7, 10, 13, and 16 m from the left screw anchor. These locations are enumerated as Target Patch #1 – #5, and mark the sites of 1 m^2 patches, where targets are deployed (dark blue patches in Fig. 2). For brevity, Target Patch numbering will be abbreviated to, for example, TP1. When seven targets are placed into the field, the additional two targets are put in 1 m^2 patches between TP2 and TP3 and TP3 and TP4 (light blue patches in Fig. 2).

Target Patches were created by the divers using a set of T-bar aluminum rails that are registered against the 11 m guide line. The T-bar aluminum rails are set perpendicular to the guide line, separated by ~ 1 m, and then driven into the sand. The rails are checked for levelness and adjusted as needed. Divers smooth the sand interface by scraping a third aluminum bar, which is perpendicular to the two T-bar rails, along these rails. Low spots are filled with sand from outside the target field, and excess sand accumulates near the front and back of the target field. The excess sand is smoothed to prevent the build up of small berms. This procedure is followed prior to a set of measurements, where a set is defined by a number of target rotations relative to mobile-tower/rail system.

To orient the targets, a square PVC frame with dimensions comparable to the target patch is utilized. One side of the frame is referenced to the 11 m guide line, which enables all four sides of the frame to encompass a Target Patch. A series of holes in the frame allowed the divers to select one of several angles. The angles used in PondEx10 for targets with cylindrical symmetry ranged from -80° to 80° in 20° increments. A target is broadside to the rail system at 0° with the nose of a UXO pointing towards the stationary tower.

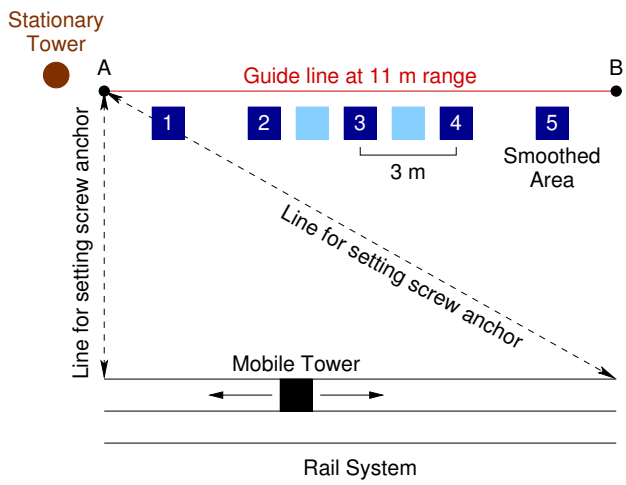

Figure 2: Schematic layout of the target field. The left and right screw anchors are denoted by 'A' and 'B'.

The nose (tail) of a UXO pointed towards the rail in the -80° (80°) orientation. For the rocks, the rotations covered -80° to 280° due to their asymmetry.

The mobile tower is placed on the rail system, and it holds acoustic sources and receivers. The mobile tower moves at 0.05 m/s with the source transmitting a ping every 0.5 s. The total distance traveled along the rail is 19 m. Thus, a SAS data set contains 760 pings, and each data set is referred to by a "sequence number". The receiver on the mobile tower is a six channel vertical array and each channel is recorded separately at a 1 MHz sample rate. The acoustic receivers located on the stationary sonar tower (see Fig. 2) were mounted on horizontal pan and vertical tilt motors. This allowed accurate alignment of the main lobe of the receivers with the Target Patches. The stationary receivers recorded data at a 500 kHz sample rate. The sources and receivers on both the rail system and stationary sonar tower stood about 4 m above the water-sand interface. When traveling from left-to-right in Fig. 2, a source transmitted a 6 ms LFM chirp centered at 16 kHz with 30 kHz of bandwidth. On the return trip, a second source transmitted a 4 ms LFM chirp centered at 40 kHz with 20 kHz of bandwidth.

Two target fields were deployed during PondEx10: one with targets at 10 m horizontal range from the rail system and one with targets at 5 m horizontal range. At a 10-m range, the targets were proud on a flattened water-sand sediment interface. The targets were either proud, half-buried, or flush buried when placed at 5 m. The 10 and 5 m ranges correspond to $\sim 20°$ and $\sim 40°$ grazing angles with respect to the source and receiver locations, respectively. The critical grazing angle for the sand in the test pond was nominally 28°. Thus, data collected for the proud targets were at shallow and steep grazing angles; while data collected for the half-buried and fully buried targets corresponded to a steep grazing angle case. When five targets were placed in the target field, the separation distance between adjacent targets was approximately 3 m. This distance was selected to minimize multiple scattering between targets. When the additional two targets were inserted into the target field, the separation distance was reduce to 1.5 m for the inner five targets.

Data Processing and Discussion

The data were initially processed using time-domain and frequency-domain synthetic aperture sonar (SAS) techniques in which high resolution images were generated. A brief description of the time-domain method follows. First, a raw SAS data set is pulse compressed by match filtering the pings with a replica of the transmitted LFM chirp. During the match filtering, a Hilbert transform converts the real-valued recorded pings to complex-valued signals. Next, baseband pulse-compressed data are obtained by multiplying by $\exp(\imath\omega_0 t)$, where ω_0 is an angular carrier frequency and our processing scheme assumes a negative time convention. Figure 3 shows the magnitude of the baseband pulse-compressed pings for sequence 27, which used the 1–31 kHz LFM chirp. This sequence included (from top to bottom in Fig. 3) the machined aluminum

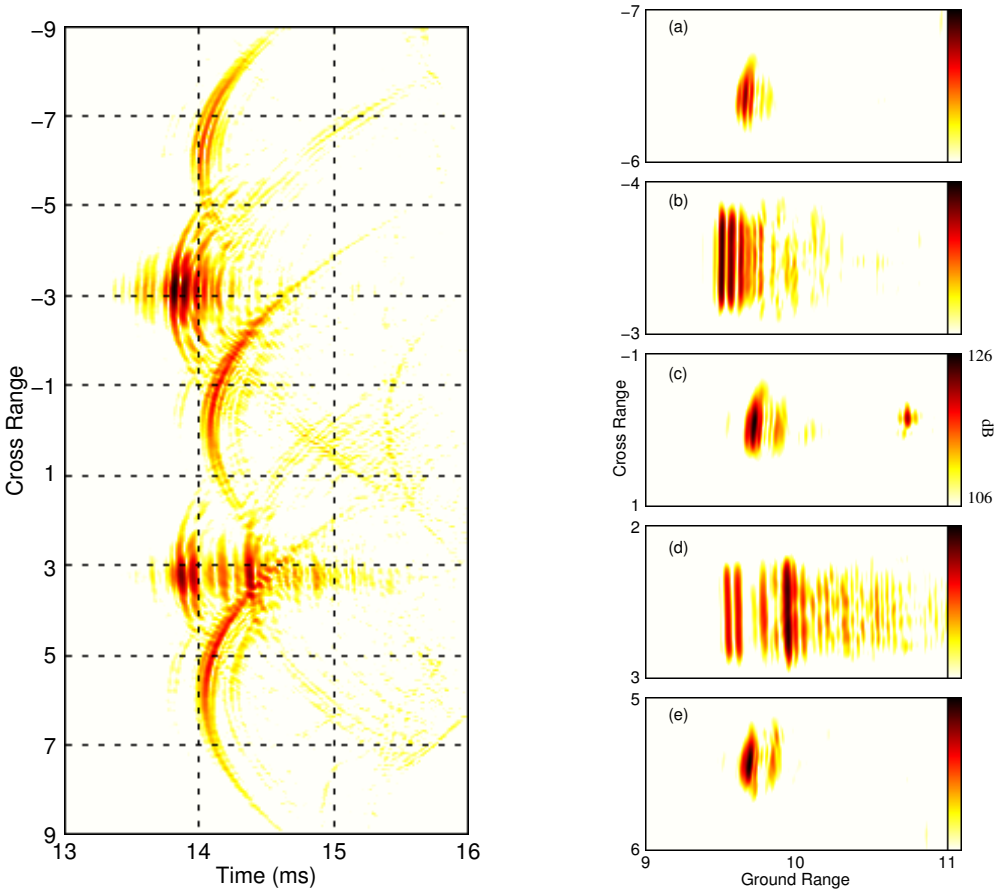

Figure 3: Left: Baseband pulse-compressed data for sequence 27. The image is normalized by the maximum value in the data and displayed on a 0 to −30 dB color scale. Right: SAS images of the targets in for sequence 27.

UXO, 2:1 solid aluminum cylinder, machined steel UXO, 2:1 aluminum pipe, and the solid artillery shell. These targets with the exception of the solid aluminum cylinder are shown in the right panel of Fig. 1. The target are proud and in a broadside orientation. It is immediately evident that the scattered acoustic field from an individual target interferes with its neighbors. The overlap of the scattered acoustic fields has an important consequence for the acoustic template processing discussed below. However, for SAS processing the coherent addition of the complex time signals is unaffected by this overlap. The next step to produce a SAS image from the time-domain data is to use a simple delay-and-sum beamformer [6]. For each pixel in a SAS image, the signals are time shifted to account for propagation from the source to the pixel and then from the pixel to the receiver. Once the time shift is performed, the signals are coherently added to determine a complex reflectivity of the pixel. This time shifting is done for each pixel in a SAS image. Images for individual channels of the receive array as well as the superposition of the six channels have been constructed.

SAS images for the targets in sequence 27 are shown on the right side of Fig. 3. These images are 1×2 m^2 patches with a 1 cm^2 pixel resolution. For Fig. 3, the six channels of the receive array have been summed. This gives a larger overall vertical aperture, and hence, a narrower main lobe for the receiving array, which limits complications due to surface reverberations and multipath arrivals. A relative dB scale is determined from the magnitude of the "loudest" pixel with the two-way spreading loss removed.

Figure 3(a) in [5] is a SAS image of the same solid aluminum cylinder obtained in the previous year's PondEx09 measurement, and it is similar to Fig. 3(b) shown here. Williams *et al.* developed an acoustic

ray model (see Fig. 5 in [5]) to understand the observed triplet structure. Briefly, the rays that contribute to this structure are:(1) a ray from the source that is directly reflected from the cylinder to the receiver; (2) a ray from the source that is reflected from the cylinder to the water-sand interface and then to the receiver; (3) a ray from the source that is reflected from the water-sand interface to the cylinder and then to the receiver; and (4) a ray from source that is reflected from the water-sand interface to the cylinder, the cylinder reflected the ray back along its incoming path to sediment and then to the receiver. The features beyond the triplet structure have been associated with the elastic response of the target.

The geometric shape of the targets in Fig. 3(a), (c), and (e) are identical. In Fig. 3(a), the triplet structure observed with the solid cylinder is again seen. Given the cylindrical symmetry of these targets, it is not unexpected to observe a similar structure. The triplet structure is not observed in (c) and (e). This may be a consequence of the "loudness" of the steel targets, the small time difference in the arrival of the four ray paths to the receiver, and the 20 dB range used to display the image. Comparison of these images also shows that the aluminum target has a much weaker feature following the main geometric response. This suggests over the frequency range of the LFM chirp, the machined aluminum UXO has a much different elastic response in comparison to the machined steel UXO and the solid steel artillery shell. Finally, in (c) the feature near 10.75 m is due to a screw anchor that was inadvertently left in the target field during the collection of sequence 27.

The final SAS image to consider is that of the aluminum pipe in Fig. 3(d). The triplet structure is no longer found and instead a doublet appears. A physical acoustics based ray model has yet to be constructed. Presumably, one or more reflection coefficients needed in the ray models for the water-filled cylindrical shell may lead to a destructive interference of some of the ray paths. The bright return at 10 m is associated with an acoustic field that is transmitted into the pipe and reflected from the far side. The other observed structure probably is due to an elastic response of the pipe. Finite element modeling of this experimental situation is an on-going task under an ONR funded projected.

The data were further processed to generate acoustic templates of the target strength as a function of frequency and aspect angle. Due to the relatively small separation distances between the UXO targets, the scattered fields from the targets overlap (see the left panel in Fig. 3). To generate an acoustic template, a novel SAS filtering technique was used to isolate the response of an individual target and to suppress reverberation noise. The details of the SAS filtering will be given elsewhere. A brief summary is as follows. The raw SAS data set is deconvolved with a target arc (i.e., point spread function) for a single selected location in an image plane, and a SAS image is formed. As an observation point in the SAS image moves away from the selected location, the image becomes defocused because the target arc is not appropriate for distant locations. The SAS image is then windowed in the spatial domain about the selected location. This windowed image contains the information to reconstruct the time signals associated with a given target via a convolution with the same target arc. It is noteworthy that the deconvolution and convolution processes are linear operations, and hence in the absences of multiple scattering the recovered signal isolates the response of the selected target.

Inspection of the target arcs in the left panel in Fig. 3 suggests that, at most, an aspect angle range for a given target in a given sequence spans approximately $\pm 15°$. This motivated the choice of target rotations from $-80°$ to $80°$ in $20°$ increments. Thus, adjacent rotation angles provide an overlap in the aspect angle ranges (e.g., $20° \pm 15°$ and $40° \pm 15°$), which permits the nine sequences to be stitched together to form acoustic templates shown in Fig. 4. The overlapping regions were determined by a cross-correlation of the aspect angle ranges for adjacent rotation angles. Once the overlap was established, the two ranges are merged by a smoothing operation over the overlap region.

A cursory inspection of Fig. 4 reveals that the structure observed for the machined steel UXO is a better match to the steel artillery than the machined aluminum UXO. In this figure, $90°$ and $270°$ correspond to a broadside orientation, $0°$ and $360°$ have the nose of the ordnance pointing at the rail system, and $180°$ corresponds to the tail pointing toward the rail. Currently, finite element models of these UXO are being constructed to investigate the observed acoustic templates. Based on the results of Williams *et al.* and Bucaro *et al.* , it is anticipated the observed differences are associated with an elastic response of the targets [4, 5].

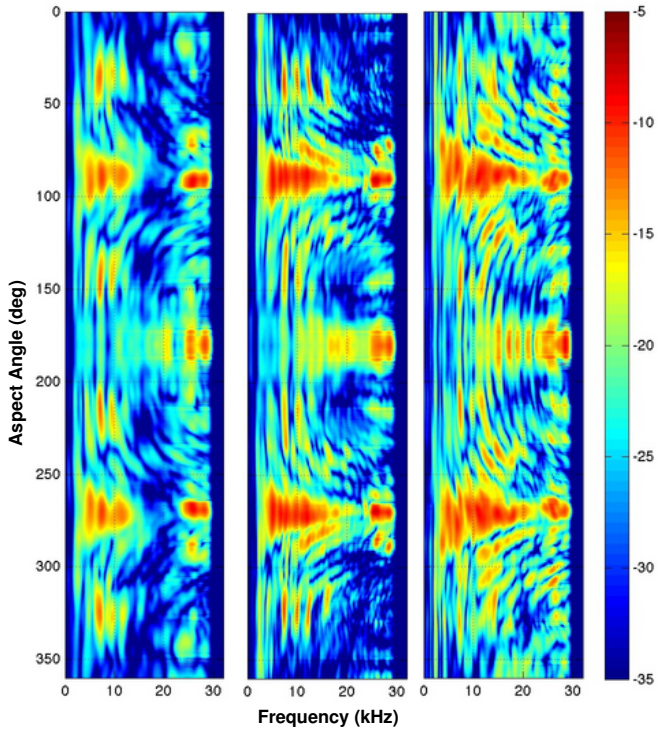

Figure 4: Acoustic template for for the machined Aluminum UXO (left), machined steel UXO (center), and (3) solid steel artillery shell (right).

Conclusion

The preliminary analysis of PondEx10 SAS data sets suggest that low frequency wide bandwidth SAS systems are capable of UXO detection and discrimination. Work remains to demonstrate that the acoustic template for a given UXO can be used as a fingerprint to uniquely identify a detected target as a UXO. The results of a finite element model analysis of the solid cylinder and partial results for the pipe have shown the complex structure found in their acoustic templates can be directly related to an elastic response of the target. Finite element models for the various UXO in our experiments are currently under construction, where it is anticipated that the structure observed in Fig. 4 may be reproduced. Finally, the current method for the construction of the acoustic templates demonstrates that the SAS filtering technique and the merging of aspect angle ranges via correlation and smoothing techniques provide a robust approach to acoustic template generation.

Acknowledgment

PondEx10 was conducted with support under SERDP projects MR-1665 and MR-1666 and with additional support from the Office of Naval Research. Dr. Joseph Lopes, Dr. Jermaine Kennedy, and Dr. Raymond Lim from NSWC PCD, and Prof. Philip Marston and Dr. Timothy Marston contributed to PondEx10 measurement, various aspects of the data analysis, and insights into the structures observed in the SAS images and acoustic templates.

References

[1] Terrence P. Long, "A global prospective on underwater munitions," *Mar. Technol. Soc. J.*, **43**, 5–10 (2009).

[2] Mike L. Overfield and Lisa C. Symons, "The use of the RUST database to inventory, monitor, and assess risk from Undersea Threats," *Mar. Technol. Soc. J.*, **43**, 33–40 (2009).

[3] Andrew Schwartz and Erika Brandeburg, "An overview of underwater technologies for operations involving underwater munitions," *Mar. Technol. Soc. J.*, **43**, 62–75 (2009).

[4] J. A. Bucaro, B. H. Houston, M. Saniga, L. R. Dragonette, T. Yoder, S. Dey, L. Kraus, and L. Carin "Broadband acoustic scattering measurements of underwater unexploded ordnance (UXO)," *J. Acoust. Soc. Am.*, **123**, 738–746 (2008).

[5] Kevin L. Williams, Steven G. Kargl, Eric I. Thorsos, David S. Burnett, Joseph L. Lopes, Mario Zampolli, and Philip L. Marston, "Acoustic scattering from a solid aluminum cylinder in contact with a sand sediment: Measurements, modeling, and interpretation," *J. Acoust. Soc. Am.*, **127**, 3356–3371 (2010).

[6] Steven G. Kargl, Kevin L. Williams, Eric I. Thorsos, and Joseph L. Lopes, "Bistatic synthetic aperture sonar measurements and preliminary analysis," in *Boundary Influences in High Frequency, Shallow Water Acoustics*, N. G. Pace and P. Blondel (Eds.), University of Bath, UK, Sept., 2005, pp. 137–143.

Appendix I: PondEx10 Data Set

Table 1 enumerates the data sets collected with five targets in the field at a 10 m horizontal range. The targets located in TP1 through TP5 are as followed: machined aluminum UXO, 2:1 solid aluminum cylinder, machined steel UXO, 2:1 aluminum pipe, and real steel artillery shell. The first column corresponds to the mobile tower moving left-to-right on the rail system with the source transmitting a 1–31 kHz LFM chirp. Column two corresponds to the right-to-left motion of the mobile tower, where the source transmitted a 30–50 kHz LFM chirp. "APL" in Table 1 denotes the sequence number assigned by APL to a monostatic SAS data set recorded on the mobile tower, the two character mnemonic is the sequence "number" used by NSWC PCD for the bistatic data sets collected by the stationary tower. The last column is the rotation angle of the proud targets with respect to the rail system. The acoustic template of Fig. 4 is constructed from "APL" data sets in the first column with the exception that the 10° is omitted. The separation distance between adjacent targets is 3 m.

Table 2 enumerates the data sets collected with seven targets in the field at a 10 m horizontal range. The targets located in TP1 through TP5 are as followed: Rock #1, 2:1 solid aluminum cylinder, machined steel UXO, 2:1 aluminum pipe, and rock #2. The machined aluminum UXO was placed between TP2 and TP3, and the real solid steel artillery shell was placed between TP3 and TP4. The separation distance between a rock and its adjacent target is 3 m while the separation distance between the other targets is 1.5 m. Due to the asymmetry of the rocks, these targets were rotated through a larger angular range. For the data sets 100°–180° only the rocks were rotated and the other targets remained at an 80° orientation. After the measurements up to180° were completed, the targets were removed and other scheduled experiments were conducted. Unfortunately, the asymmetry of the rocks required additional angular rotations to cover the entire 360° range. Rocks #1 and #2 were placed in TP1 and TP2, respectively, and no other targets are present. The sequence numbers 433–447 were then recorded. Finally, bistatic data were not collected during this final set of rotation measurements.

Williams *et al.* noted that the scattering for a proud target may be dependent on the phase of the sediment's reflection coefficient [5]. To remove this sensitivity from several sets of measurements, two plexi-plates were placed in TP4 and TP5. The reflection coefficient of plexi-glass is well-known and not subject to variation. These plates had octagonal shapes because the corners were removed to prevent scattering from the 90° corners. Initially, the 2:1 solid aluminum cylinder and aluminum pipe were used as reference targets. The sequence numbers for data recorded at various rotation angles are listed in Table 3. The first entry is a background from the plates alone (which would permit background subtraction of any scattering from the plates). In these initial measurements, an edge of the plates was aligned parallel to the rail system, and it produced a strong feature in the SAS images. The scattering from the edge is not easily removed from the baseband pulse-compressed time signals, so the plates were rotated by 22°, which points a corner of the octagon at the rail system. The sequence numbers for a second set of measurements after the plate rotation are given in Table 4.

Once the data sets from the reference targets were collected, the aluminum cylinder and pipe were replaced by the machined aluminum UXO in TP4 and by the machined steel UXO in TP5. The data sets are listed in Table 5. With the known reflection coefficient for the plexi-glass and the identical target shapes, these measurements allow one to investigate the importance of an elastic response from the targets. These data sets, combined with on-going finite element modeling of the target response, should yield an unambiguous understanding of the scattering from this particular target shape.

At this point in PondEx10, the 152 mm TP-T round was acquired along with a 155 mm howitzer projectile, which contained plaster and ethylene glycol mixture. Due to the ethylene glycol, NSWC PCD environmental and safety office would not approve the deployment of the 155 mm howitzer projectile in the pond. A series of measurements were conducted with the 152 mm TP-T round, small aluminum cylinder with a notch, the steel artillery shell, an 81 mm mortar, and the machined aluminum UXO while a replacement for the howitzer projectile projectile was secured. Tables 6, 7, and 8 list the sequence numbers for the measurements that were conducted for proud targets, 1/2 buried targets, and fully buried targets, respectively.

After the data in Tables 6, 7, and 8 were collected the targets were removed from the target field and other scheduled measurements were carried out. Upon receiving a replacement 155 mm howitzer projectile, a new target field was prepared by the divers at the 10 m range. The light blue areas in Fig. 2 were filled with sand and the divers flattened these areas and the target patches (dark blue) with hand trowels. The divers also removed berms that accumulated at the rear of the target. Six targets were deployed with the 152 mm TP-T round in TP2, the steel artillery shell in TP3, an 81 mm mortar in TP4, the 155 mm howitzer projectile in TP5, the small aluminum cylinder with a notch between TP2 and TP3, and the machined aluminum UXO between TP3 and TP4. The separation distance between adjacent targets is 1.5 m. Tables 9, 10, and 11 list the sequence numbers for the measurements that were conducted for proud targets, 1/2 buried targets, and fully-buried targets, respectively.

Tables 12 and 13 contain the data sequence numbers for experiments conducted in a target field that was 5 m from the rail system. The target field at 5 m was prepared by the divers in the same manner as the 10 m target field. These measurements augment those conducted during PondEx09 at a 40° grazing angle for proud and fully-buried targets. During PondEx09, neither the 152 mm TP-t round, the 155 mm howitzer projectile, nor machined aluminum UXO were available.

1–30 kHz		30–50 kHz		Angle	1–30 kHz		30–50 kHz		Angle
APL	NSWC	APL	NSWC	(Deg)	APL	NSWC	APL	NSWC	(Deg)
27	AI	28	AK	0	37	AS	38	AR	80
41	AK	30	AL	10	39	AU	40	AV	-20
31	AM	32	AN	20	41	AW	42	AX	-40
33	AO	34	AP	40	43	AY	44	AZ	-60
35	AQ	36	AR	60	45	BA	46	BB	-80

Table 1: Data sets for five proud targets in the 10 m target field. The data set at $\sim 10°$ was an incorrect target alignment due to the divers first experience with the new alignment frame.

1–30 kHz		30–50 kHz		Angle	1–30 kHz		30–50 kHz		Angle
APL	NSWC	APL	NSWC	(Deg)	APL	NSWC	APL	NSWC	(Deg)
47	BC	48	BD	-80	66	BV			120 †
49	BE	50	BF	-60	67	BW			140 †
51	BG	52	BH	-40	68	BX			160 †
53	BI	54	BJ	-20	69	BY			180 †
55	BK	56	BL	0	433		434		200 ‡
57	BM	58	BN	20	436		438		220 ‡
59	BO	60	BP	40	440		441		240 ‡
61	BQ	62	BR	60	443		444		260 ‡
63	BS	64	BT	80	446		447		280 ‡
65	BU			100 †					

Table 2: Data sets for seven proud targets in the 10 m target field. † Only the rocks were rotated. ‡ Final set of rotations for the rocks

1–30 kHz		30–50 kHz		Angle	1–30 kHz		30–50 kHz		Angle
APL	NSWC	APL	NSWC	(Deg)	APL	NSWC	APL	NSWC	(Deg)
74	CB	75	CC	†	80	CH	81	CI	40
76	CD	77	CE	0	82	CJ	83	CK	60
78	CF	79	CG	20	84	CL	85	CM	80

Table 3: Data sets for the 2:1 solid aluminum cylinder and pipe on plexi-glass plates. † No targets were on the plates for a background data set.

1–30 kHz		30–50 kHz		Angle	1–30 kHz		30–50 kHz		Angle
APL	NSWC	APL	NSWC	(Deg)	APL	NSWC	APL	NSWC	(Deg)
86	CN	87	CC	†	92	CT	93	CI	40
88	CP	89	CE	0	94	CV	95	CK	60
90	CR	91	CG	20	96	CW	97	CM	80

Table 4: Data sets for 2:1 solid aluminum cylinder and pipe on plexi-glass plates. Plates rotated 22° to suppress glint from edge scattering. † No targets were on the plates for a background data set.

1–30 kHz		30–50 kHz		Angle	1–30 kHz		30–50 kHz		Angle
APL	NSWC	APL	NSWC	(Deg)	APL	NSWC	APL	NSWC	(Deg)
98	CZ	99	DA	0	111	DJ	112	DK	-20
100	DB	101	DC	20	113	DL	114	DM	-40
102	DD	103	DE	40	117	DN	118	DO	-60
104	DF	105	DG	60	119	DP	120	DQ	-80
106	DH	107	DI	80					

Table 5: Data sets for machined aluminum UXO and machined steel UXO on plexi-glass plates. Plates rotated 22° to suppress glint from edge scattering.

1–30 kHz		30–50 kHz		Angle	1–30 kHz		30–50 kHz		Angle
APL	NSWC	APL	NSWC	(Deg)	APL	NSWC	APL	NSWC	(Deg)
185	EH	186	EI	0 †	195	ER	196	ES	0
187	EJ	188	EK	-80	197	ET	198	EU	20
189	EL	190	EM	-60	199	EV	200	EW	40
191	EN	192	EO	-40	201	EX	202	EY	60
193	EP	194	EQ	-20	203	EZ	204	FA	80

Table 6: Data sets for the following five proud targets at a 10 m range: small aluminum cylinder with a notch, 152 mm TP-T round, steel artillery shell, 81 mm mortar, and machined aluminum UXO. Initial data set was used to check the source level, and requires a factor of 2 compensation.†

1–30 kHz		30–50 kHz		Angle	1–30 kHz		30–50 kHz		Angle
APL	NSWC	APL	NSWC	(Deg)	APL	NSWC	APL	NSWC	(Deg)
205	FB	206	FC	-80	215	FL	216	FM	20
207	FD	208	FE	-60	217	FN	218	FO	40
209	FF	210	FG	-40	219	FP	220	FQ	60
211	FH	212	FI	-20	221	FR	222	FS	80
213	FJ	214	FK	0					

Table 7: Data sets for the following five 1/2 buried targets at a 10 m range: small aluminum cylinder with a notch, 152 mm TP-T round, steel artillery shell, 81 mm mortar, and machined aluminum UXO.

1–30 kHz		30–50 kHz		Angle	1–30 kHz		30–50 kHz		Angle
APL	NSWC	APL	NSWC	(Deg)	APL	NSWC	APL	NSWC	(Deg)
223	FT	224	FU	0	233	GD	234	GE	80
225	FV	226	FW	-20	235	GF	236	GG	-40
227	FX	228	FY	20	237	GH	238	GI	-60
241	FZ	230	GA	40	239	GJ	240	GK	-80
231	GB	232	GC	60					

Table 8: Data sets for the following five fully-buried targets at a 10 m range: small aluminum cylinder with notch, 152 mm TP-T round, steel artillery shell, 81 mm mortar, and machined aluminum UXO.

1–30 kHz		30–50 kHz		Angle	1–30 kHz		30–50 kHz		Angle
APL	NSWC	APL	NSWC	(Deg)	APL	NSWC	APL	NSWC	(Deg)
241	GL	242	GM	†	253	GX	254	GY	0
243	GN	244	GO	†	255	GZ	256	HA	20
245	GP	246	GQ	-80	257	HB	258	HC	40
247	GR	248	GS	-60	259	HD	260	HE	60
249	GT	250	GU	-40	261	HF	262	HG	80
251	GV	252	GW	-20					

Table 9: Data sets for the following six proud targets at a 10 m range: 152 mm TP-T round, steel artillery shell, 81 mm mortar, 155 mm howitzer projectile, small aluminum cylinder with a notch between TP2 and TP3, and the machined aluminum UXO between TP3 and TP4. † Background run.

1–30 kHz		30–50 kHz		Angle	1–30 kHz		30–50 kHz		Angle
APL	NSWC	APL	NSWC	(Deg)	APL	NSWC	APL	NSWC	(Deg)
263	HH	264	HI	80	273	HR	274	HS	-20
265	HJ	266	HK	60	275	HT	276	HU	-40
267	HL	268	HM	40	277	HV	278	HW	-60
269	HN	270	HO	20	279	HX	280	HY	-80
271	HP	272	HQ	0	281	HZ	282	IA	-80 †

Table 10: Data sets for the following six 1/2 buried targets at a 10 m range: 152 mm TP-T round, steel artillery shell, 81 mm mortar, 155 mm howitzer projectile, small aluminum cylinder with a notch between TP2 and TP3, and the machined aluminum UXO between TP3 and TP4. † Targets settled overnight in field.

1–30 kHz		30–50 kHz		Angle	1–30 kHz		30–50 kHz		Angle
APL	NSWC	APL	NSWC	(Deg)	APL	NSWC	APL	NSWC	(Deg)
283	IB	284	IC	-80	413	IL	414	IM	0 †
285	ID	286	IE	-60	415	IN	416	IO	20
287	IF	288	IG	-40	417	IP	418	IQ	40
289	IH	410	II	-20	419	IR	300	IS	60
411	IJ	412	IK	0	301	IT	302	IU	80

Table 11: Data sets for the following six fully-buried targets at a 10 m range: 152 mm TP-T round, steel artillery shell, 81 mm mortar, 155 mm howitzer projectile, small aluminum cylinder with a notch between TP2 and TP3, and the machined aluminum UXO between TP3 and TP4. † Targets settled over Sunday.

1–30 kHz		30–50 kHz		Angle	1–30 kHz		30–50 kHz		Angle
APL	NSWC	APL	NSWC	(Deg)	APL	NSWC	APL	NSWC	(Deg)
363 ∗		364 ∗			365 †	JU	366†	JV	
367	JW	368	JX	-80	379	KI	380	KJ	20
369	JY	370	JZ	-60	381 ‡	KK	382	KL	40
371	KA	372	KB	-60	383	KM	384	KN	40
373	KC	374	KD	-40	385	KO	386	KP	60
375	KE	376	KF	-20	387	KQ	388	KR	80
377	KG	378	KH	0					

Table 12: Data sets for the following five proud targets at a 5 m range: small aluminum cylinder with a notch, 152 mm TP-T round, machined aluminum UXO, 81 mm mortar, 155 mm howitzer projectile. ∗ Target field was not smoothed, and the 152 mm TP-T round was in TP3. † Background run after the divers prepared the target field. ‡ Data set contains a 5 second of dead time at ping 400.

1–30 kHz		30–50 kHz		Angle	1–30 kHz		30–50 kHz		Angle
APL	NSWC	APL	NSWC	(Deg)	APL	NSWC	APL	NSWC	(Deg)
391	KU	392	KV	60	401	LE	402	LF	-40
393	KW	394	KX	40	403	LG	404	LH	-60
395	KY	396	KZ	20	405	LI	406	LJ	-80
397	LA	398	LB	0					

Table 13: Data sets for the following five fully-buried targets at a 5 m range: small aluminum cylinder with a notch, 152 mm TP-T round, machined aluminum UXO, 81 mm mortar, 155 mm howitzer projectile.

Appendix II: PondEx10 SAS Images

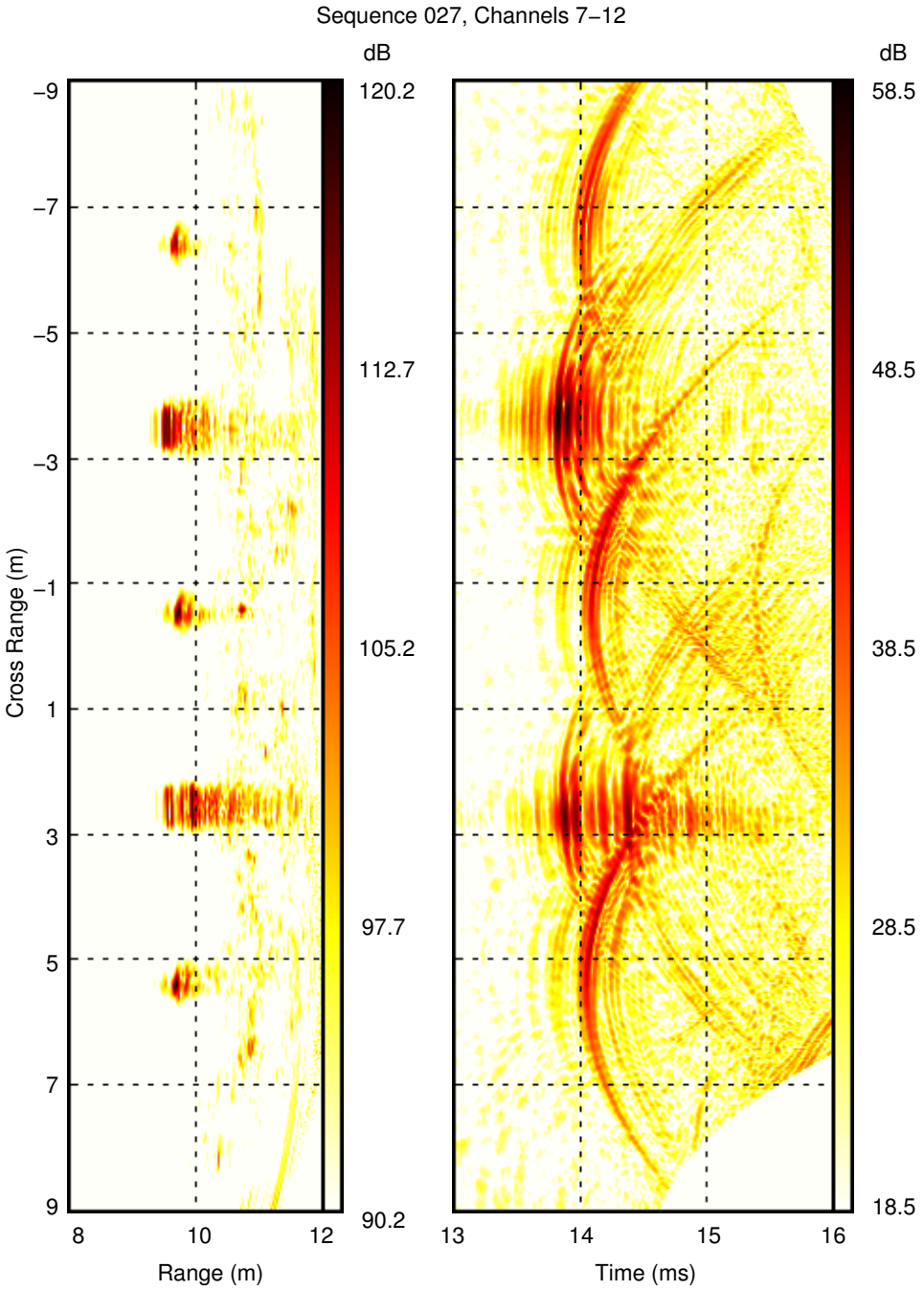

Figure 5: SAS image (left) generated from the pulse-compressed baseband time signals (right) for sequence 27. These images corresponds to the images in Fig. 3.

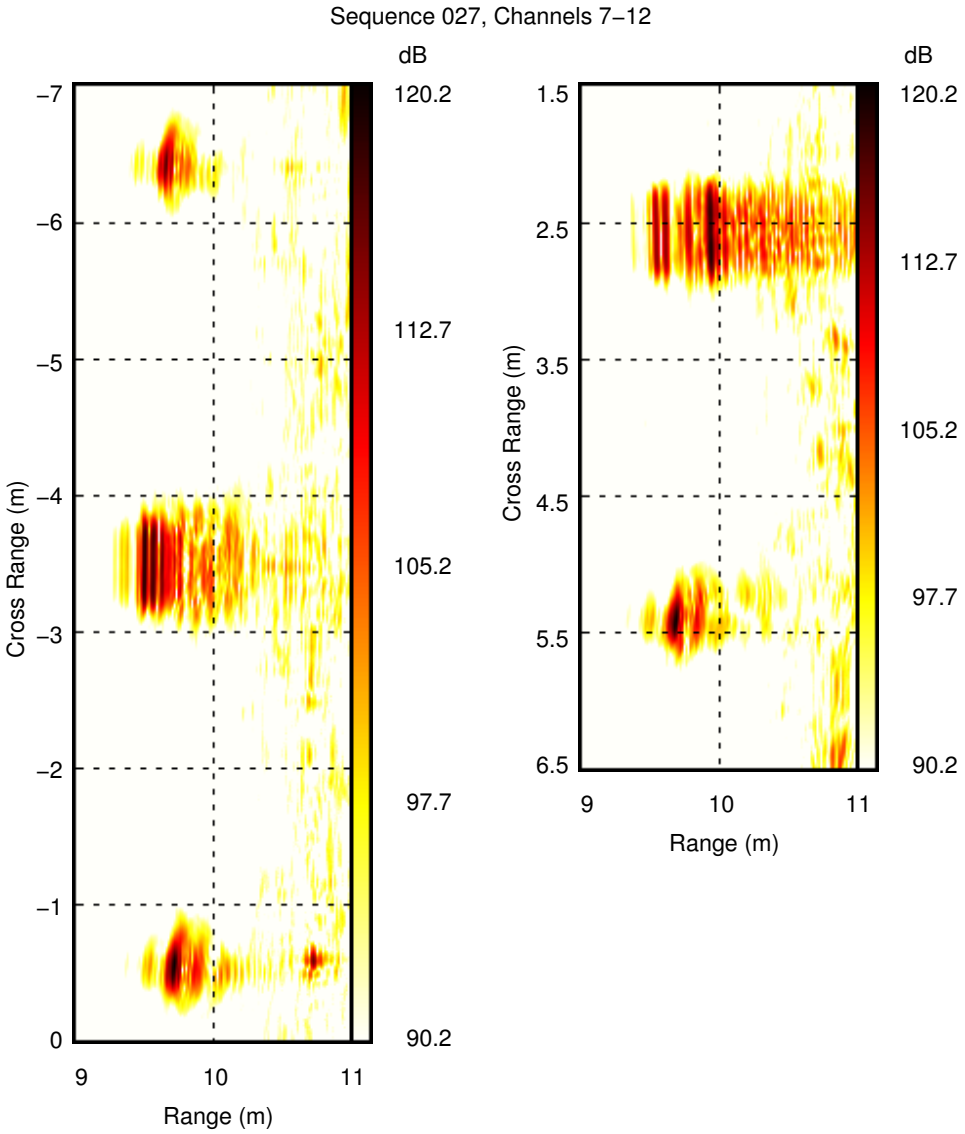

Figure 6: Higher resolution SAS image for sequence 27.

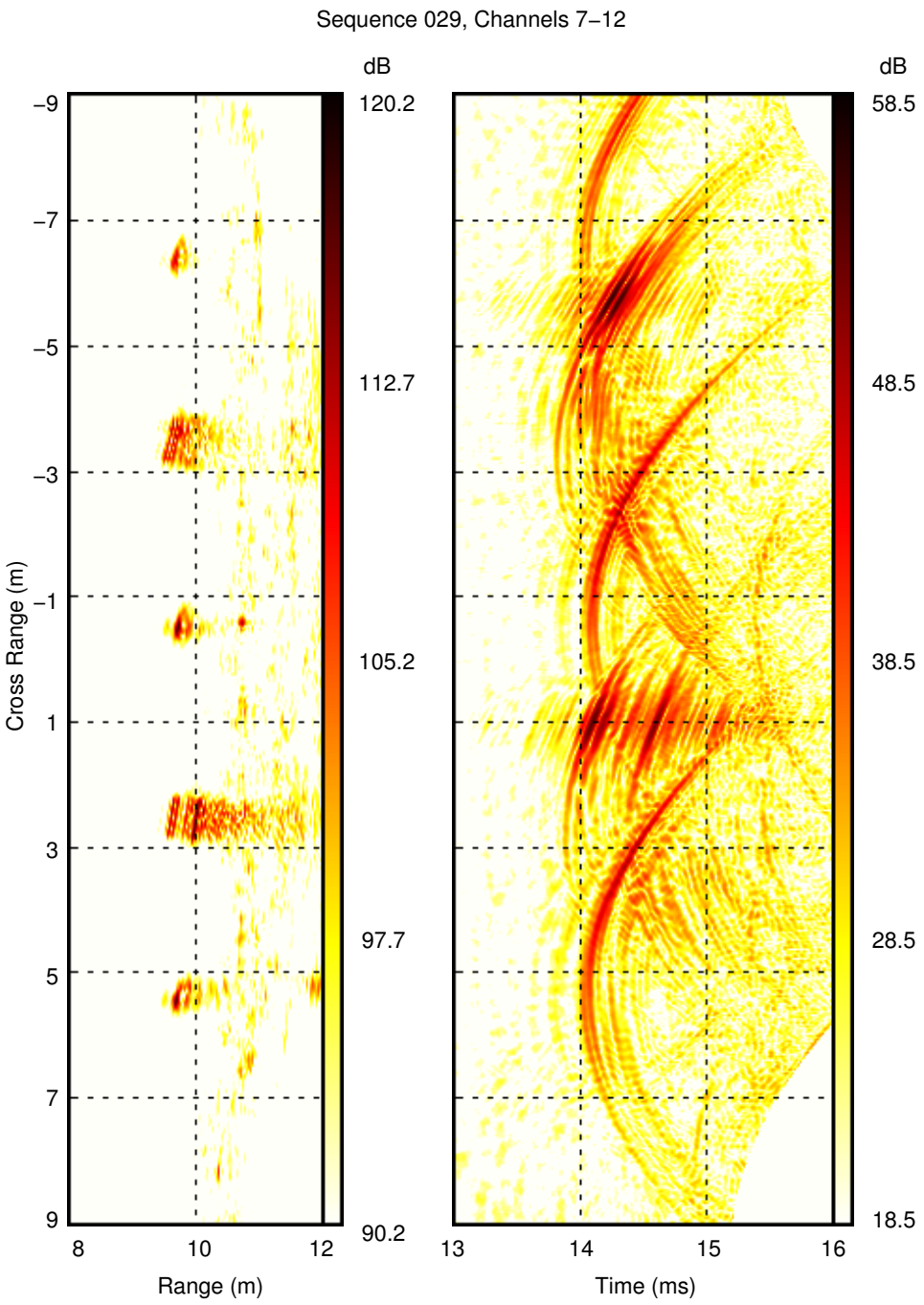

Figure 7: SAS image (left) generated from the pulse-compressed baseband time signals (right) for sequence 29.

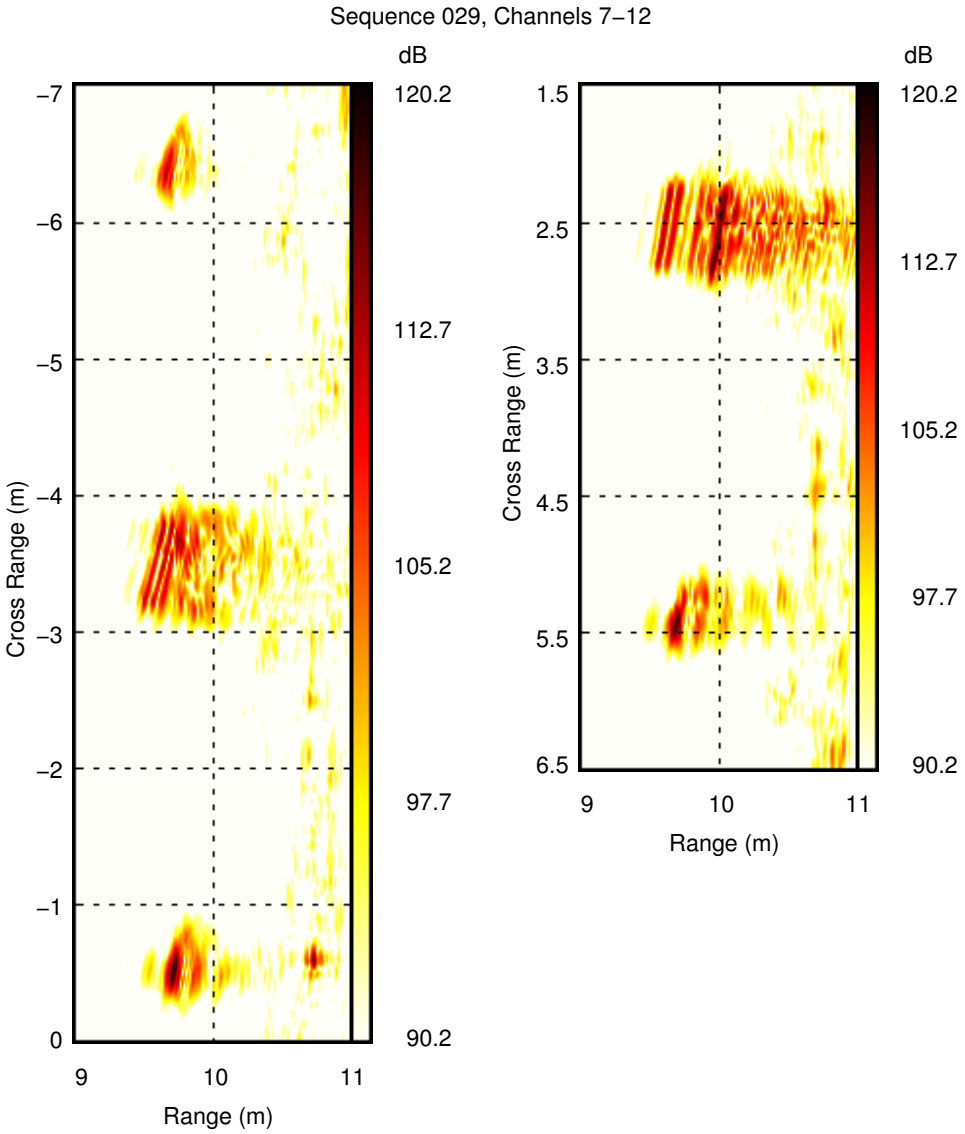

Figure 8: Higher resolution SAS image for sequence 29.

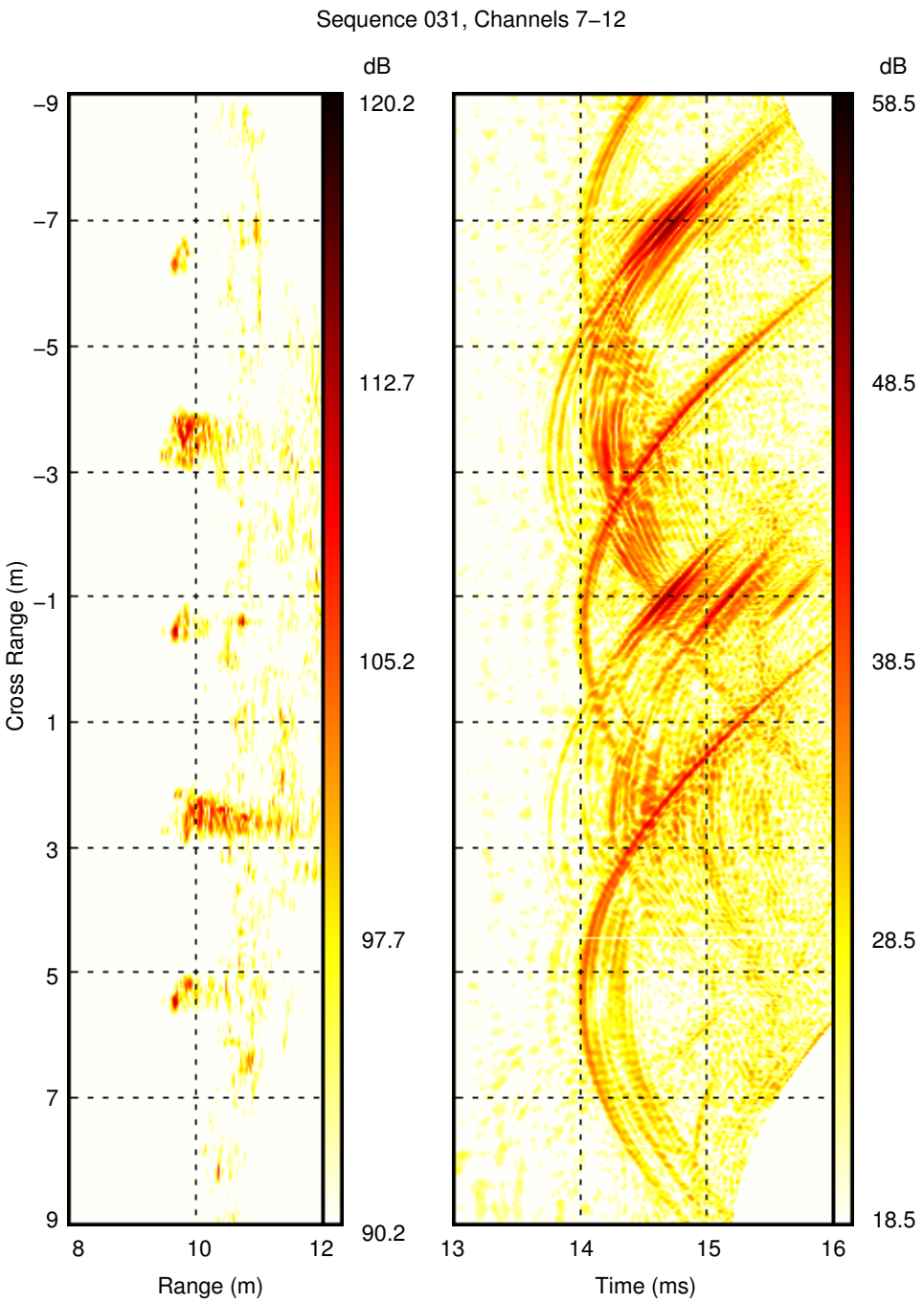

Figure 9: SAS image (left) generated from the pulse-compressed baseband time signals (right) for sequence 31.

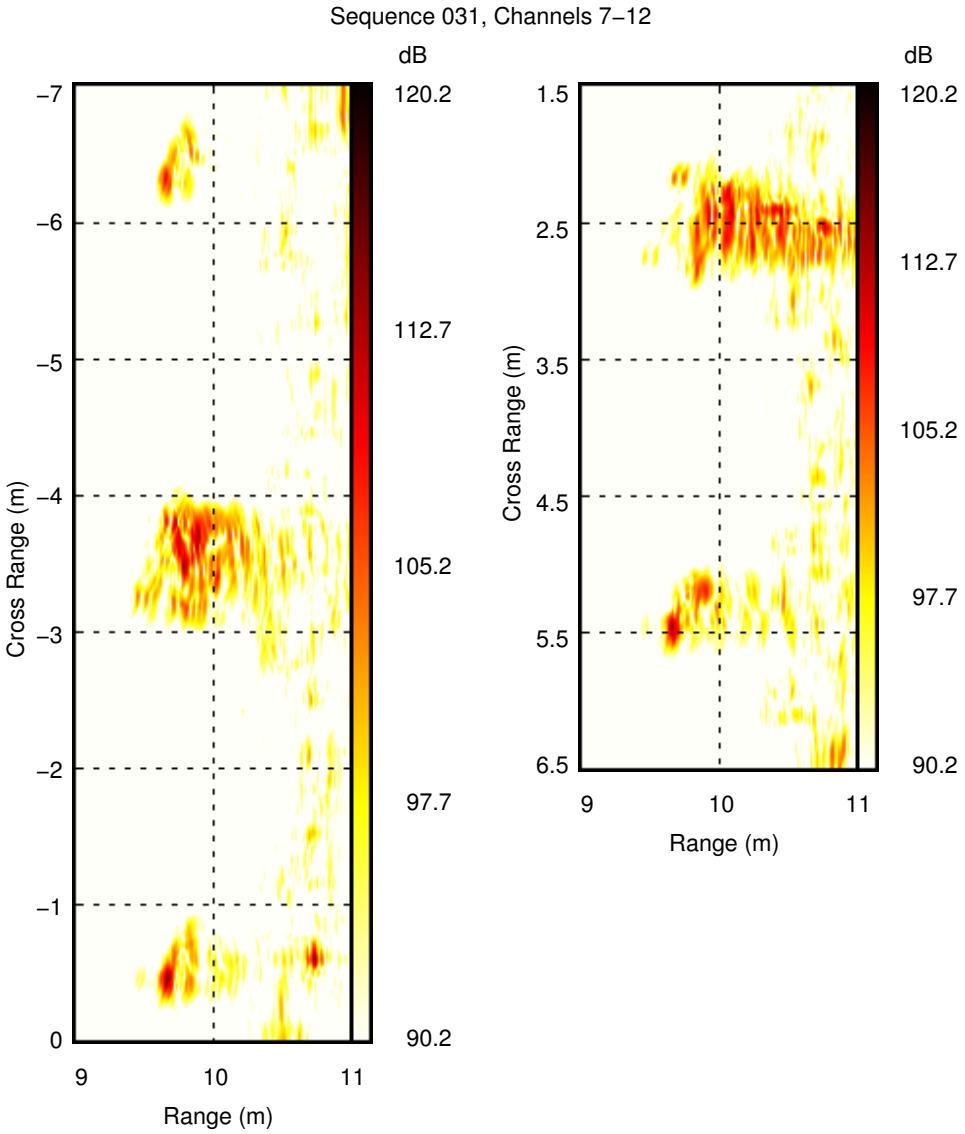

Figure 10: Higher resolution SAS image for sequence 31.

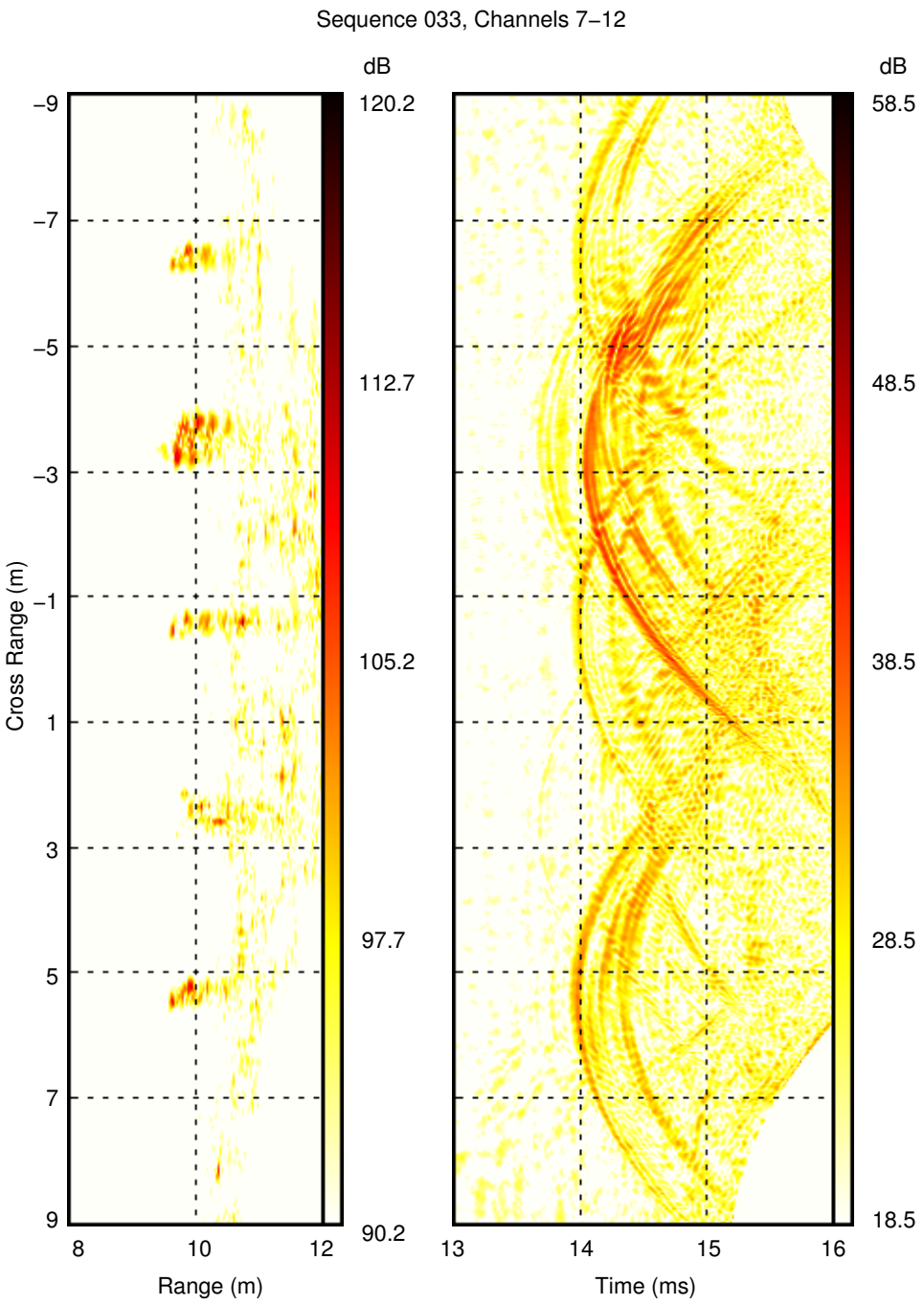

Figure 11: SAS image (left) generated from the pulse-compressed baseband time signals (right) for sequence 33.

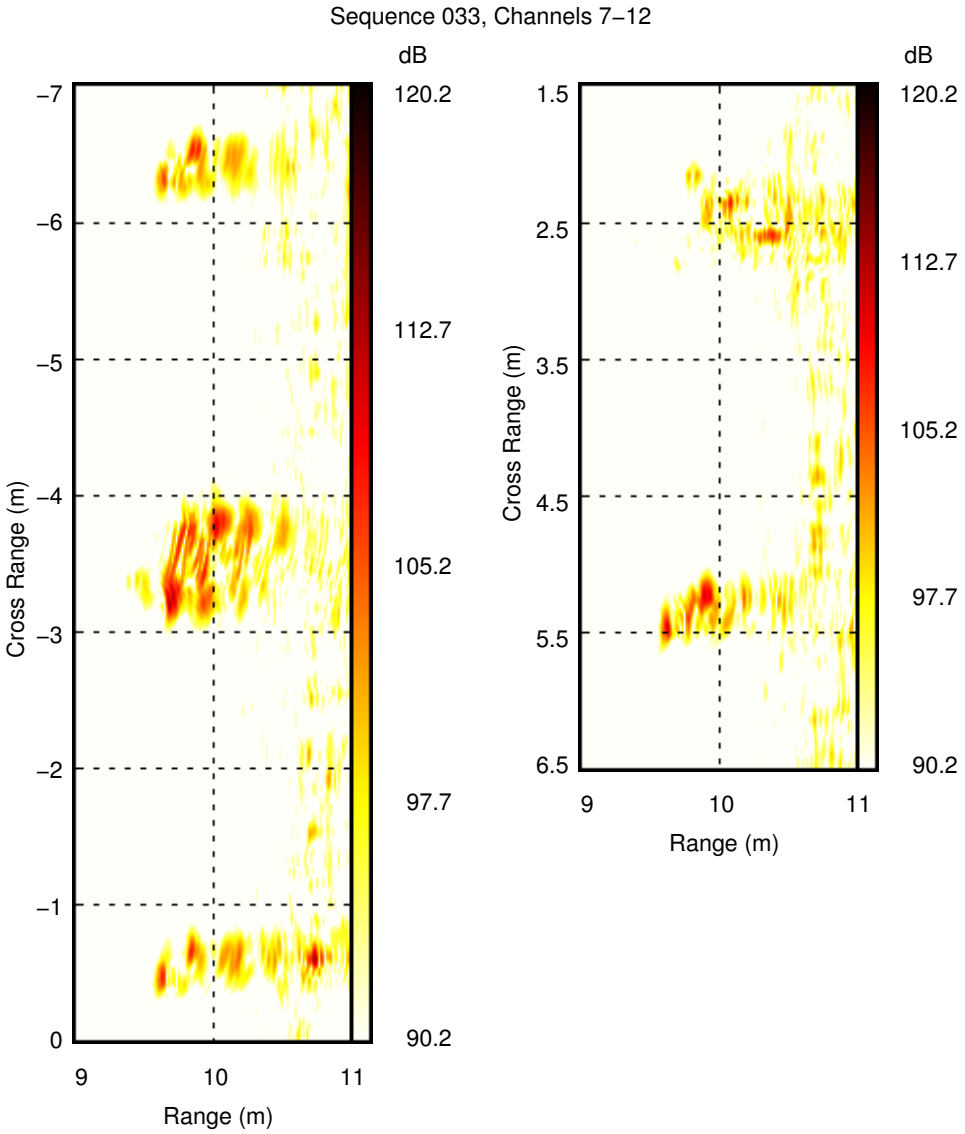

Figure 12: Higher resolution SAS image for sequence 33.

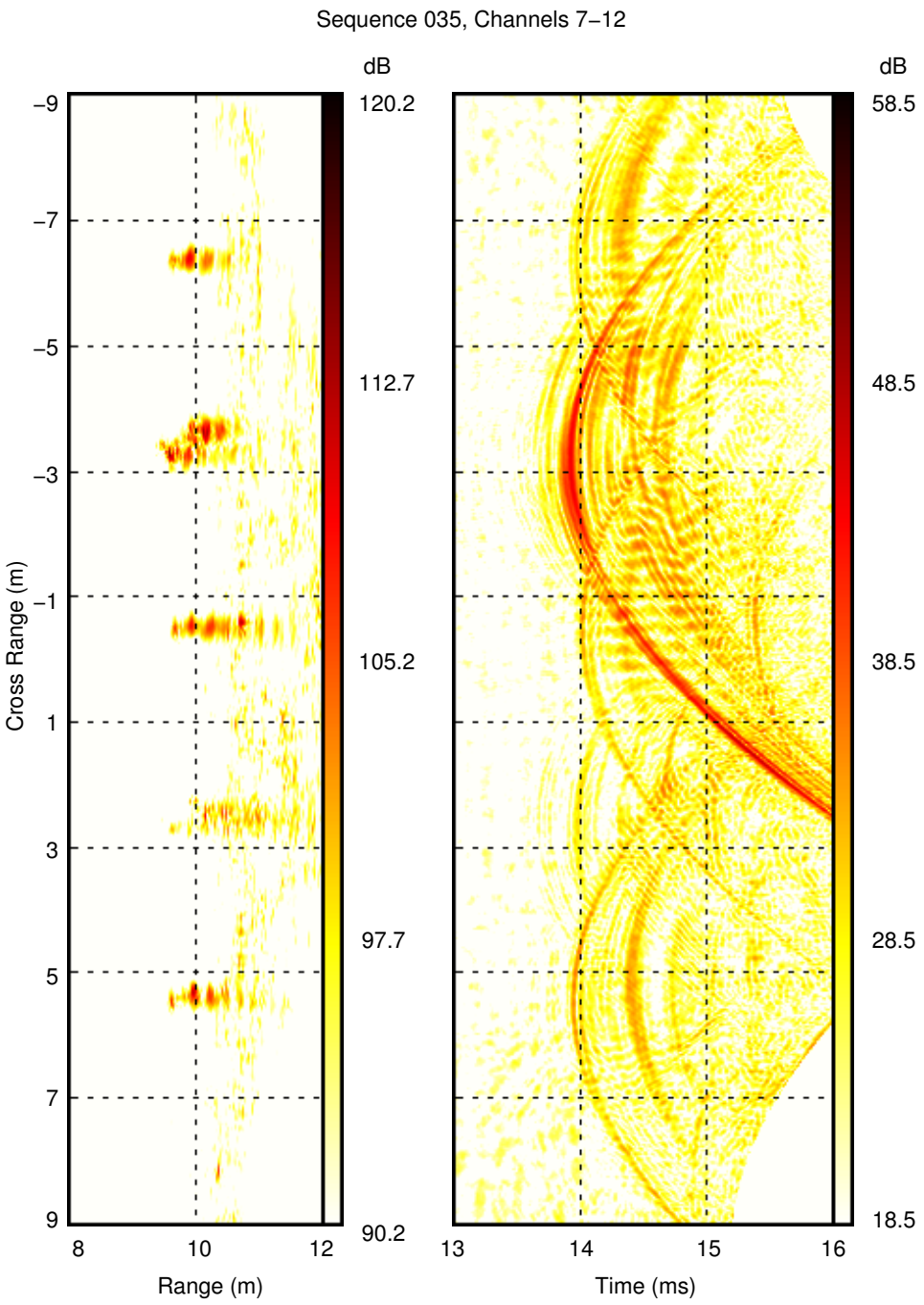

Figure 13: SAS image (left) generated from the pulse-compressed baseband time signals (right) for sequence 35.

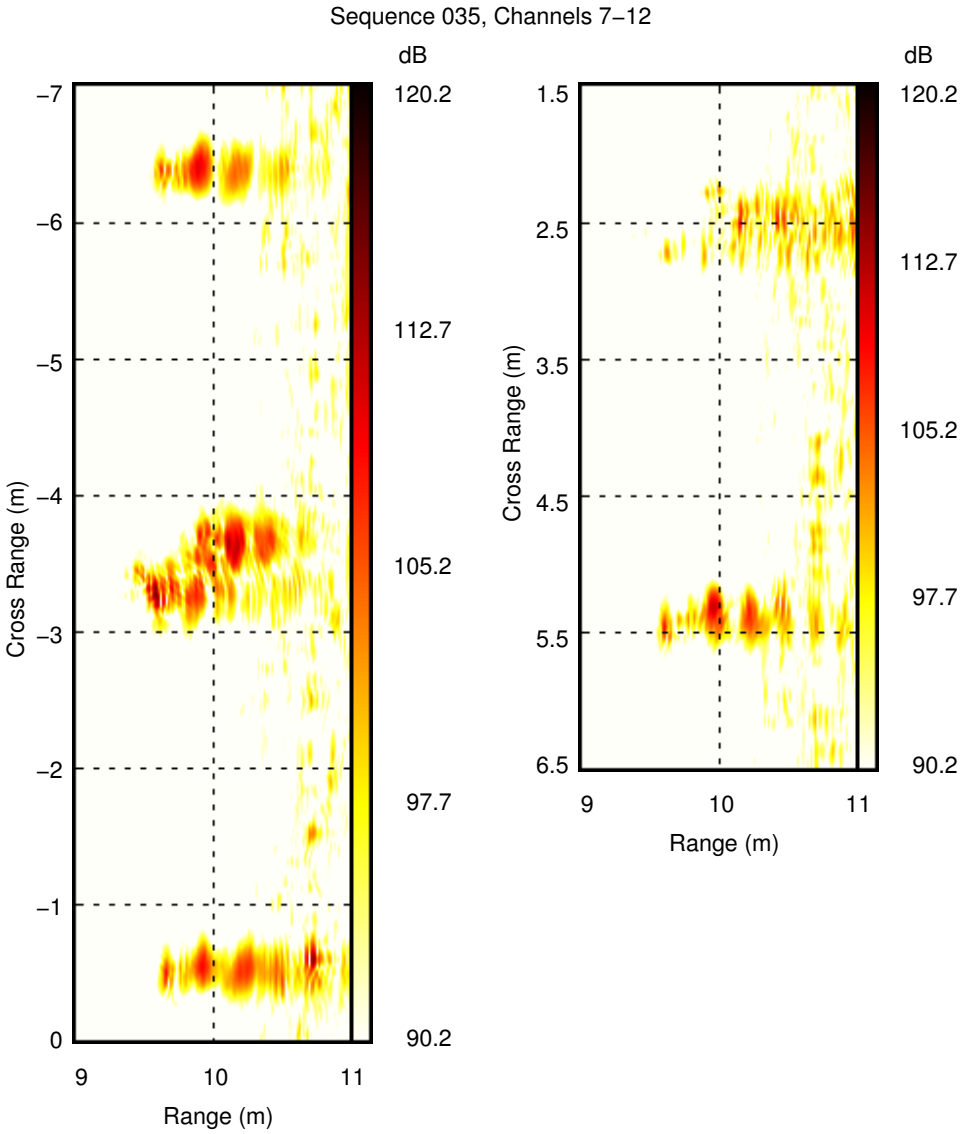

Figure 14: Higher resolution SAS image for sequence 35.

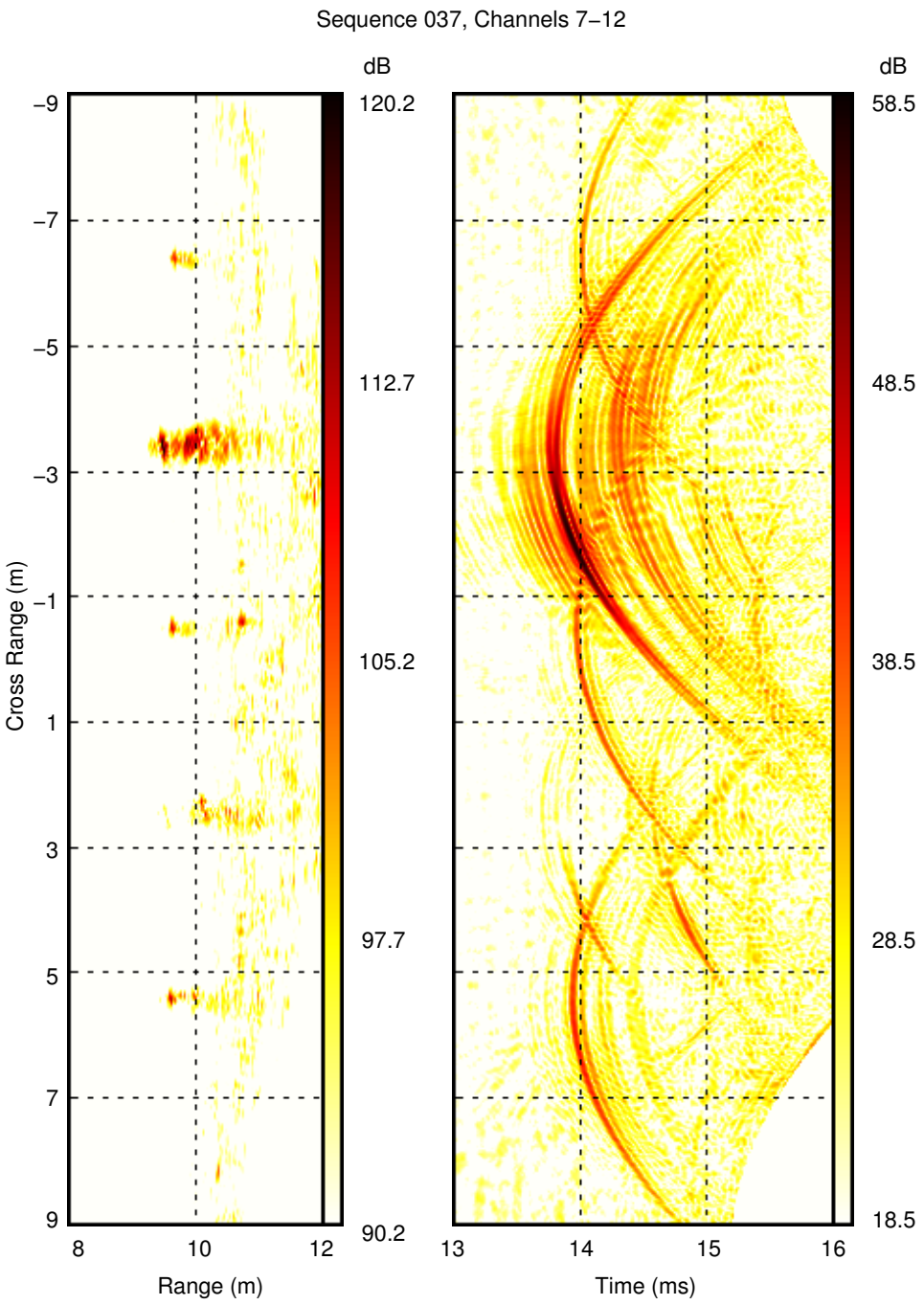

Figure 15: SAS image (left) generated from the pulse-compressed baseband time signals (right) for sequence 37.

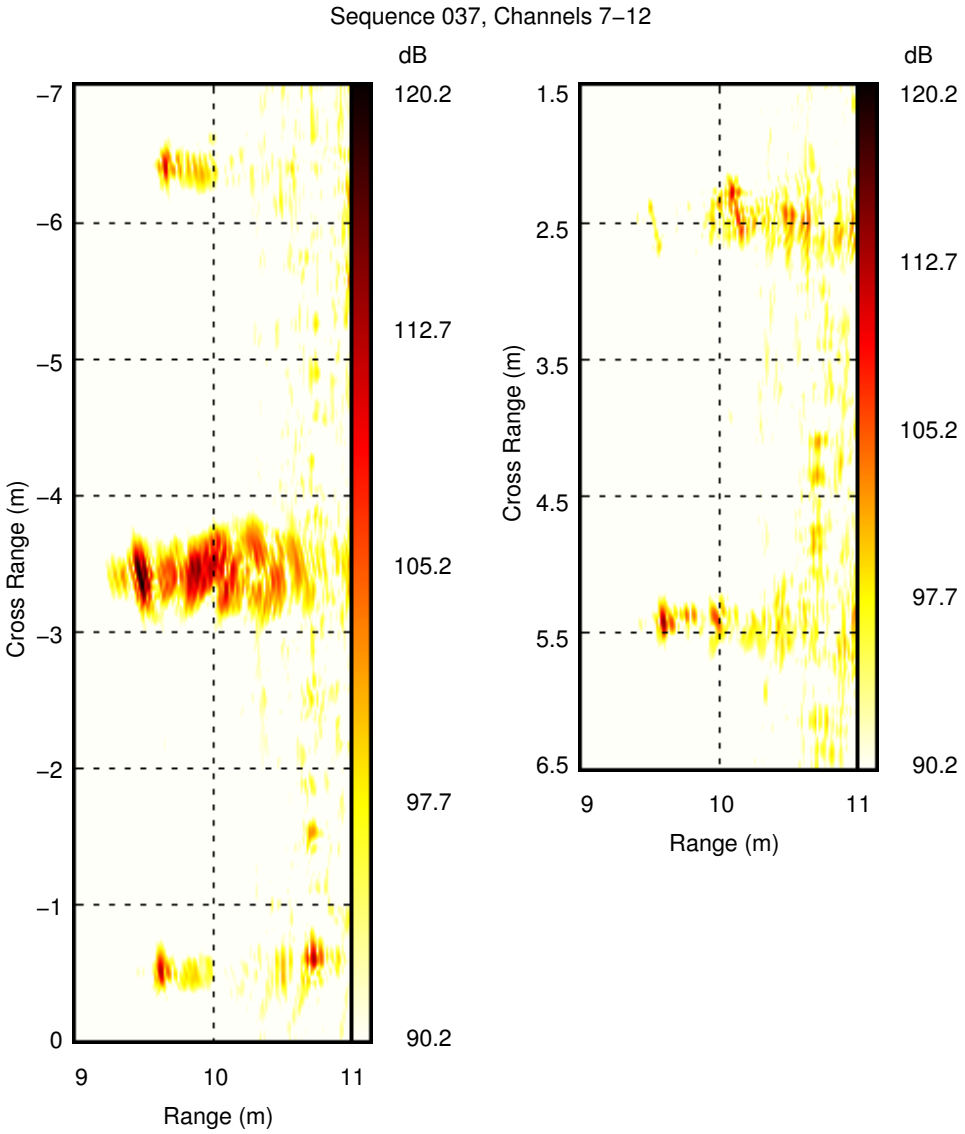

Figure 16: Higher resolution SAS image for sequence 37.

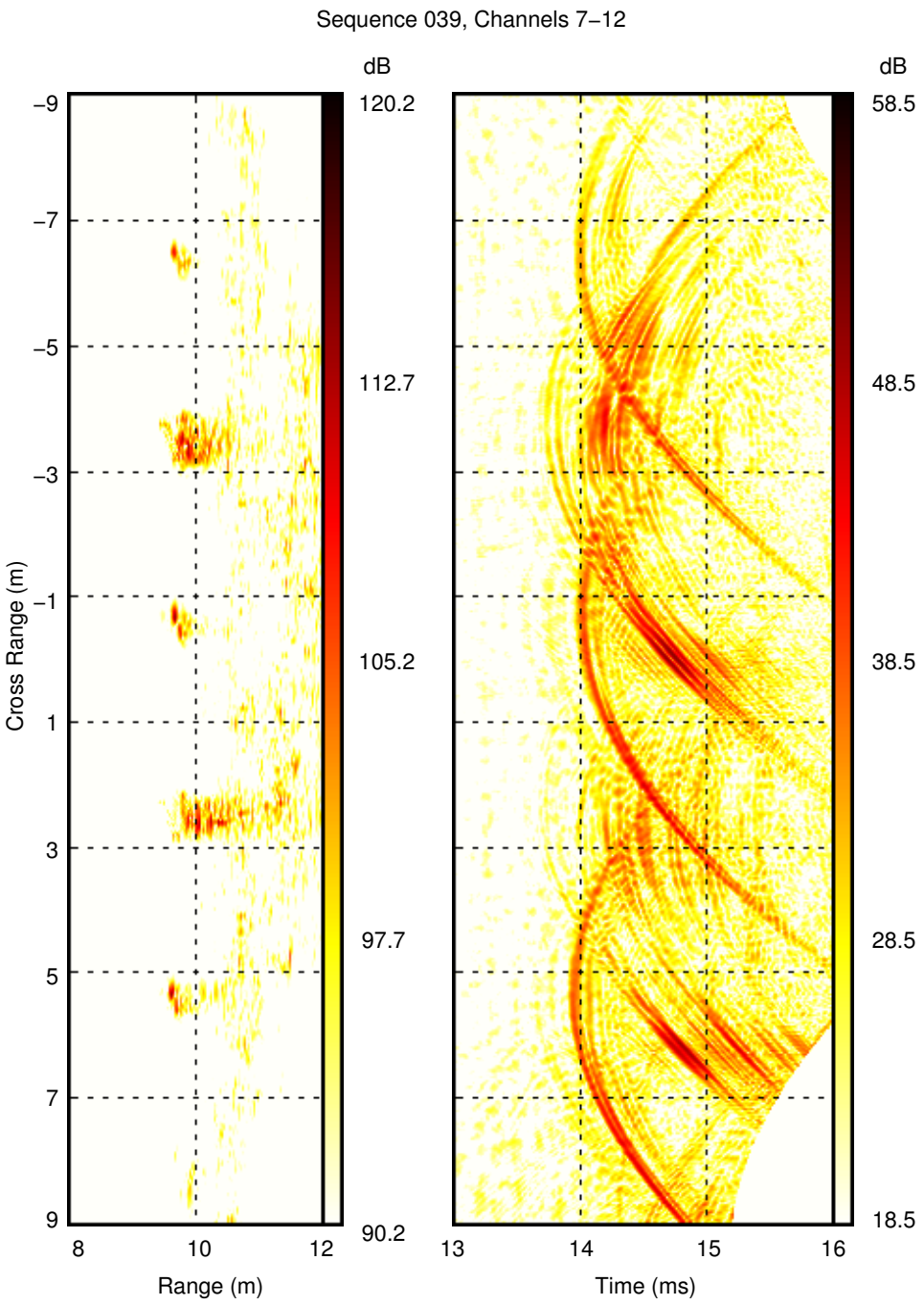

Figure 17: SAS image (left) generated from the pulse-compressed baseband time signals (right) for sequence 39.

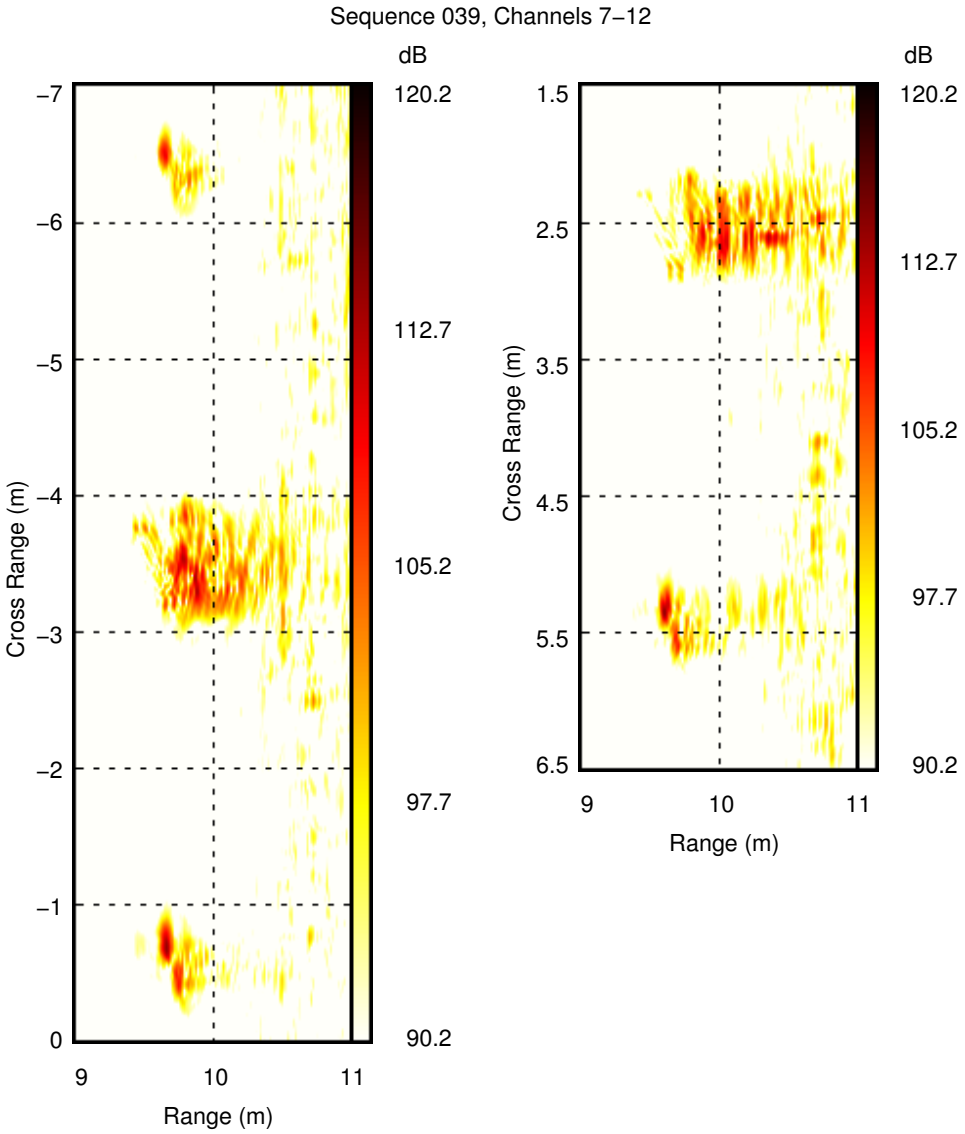

Figure 18: Higher resolution SAS image for sequence 39.

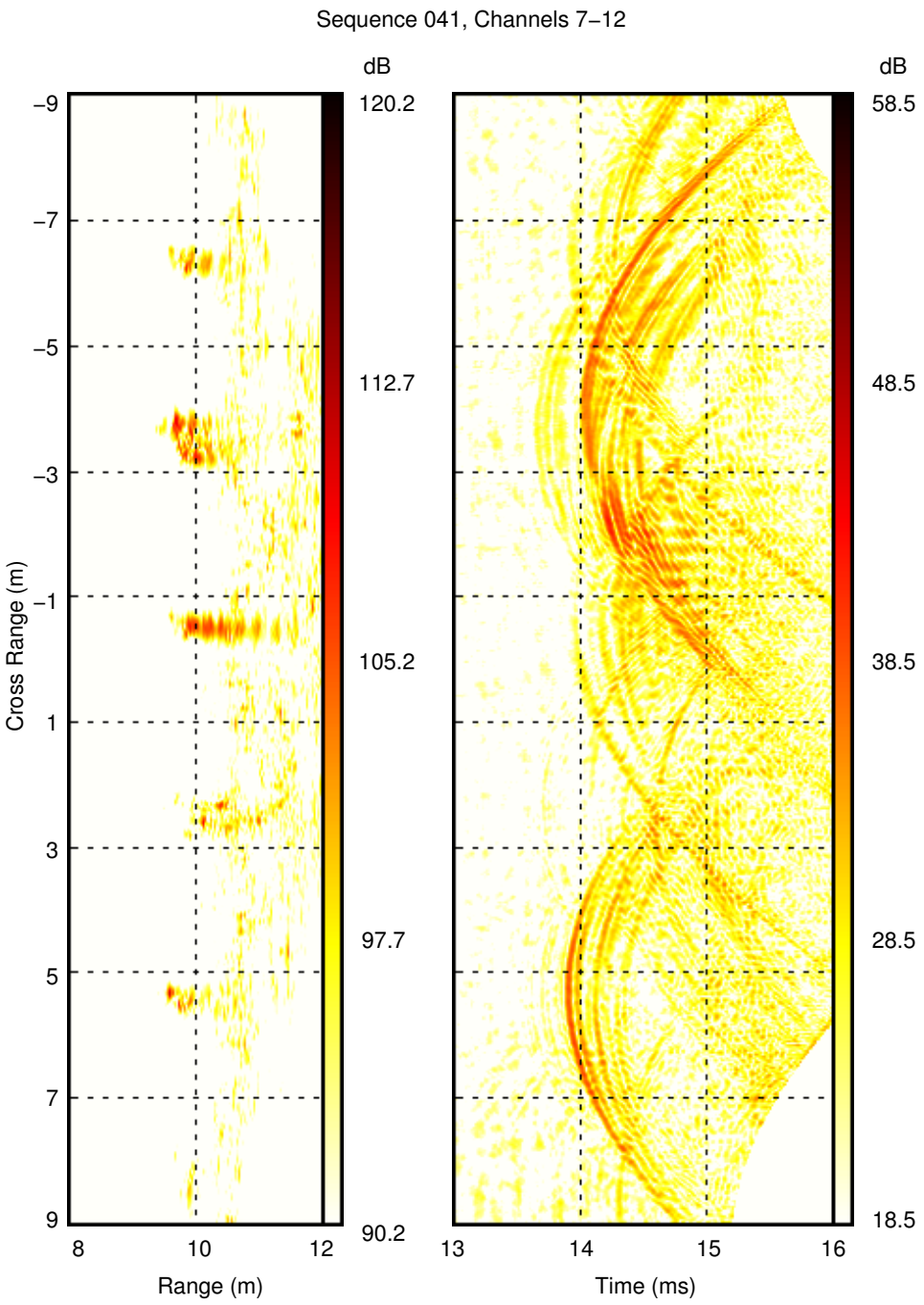

Figure 19: SAS image (left) generated from the pulse-compressed baseband time signals (right) for sequence 41.

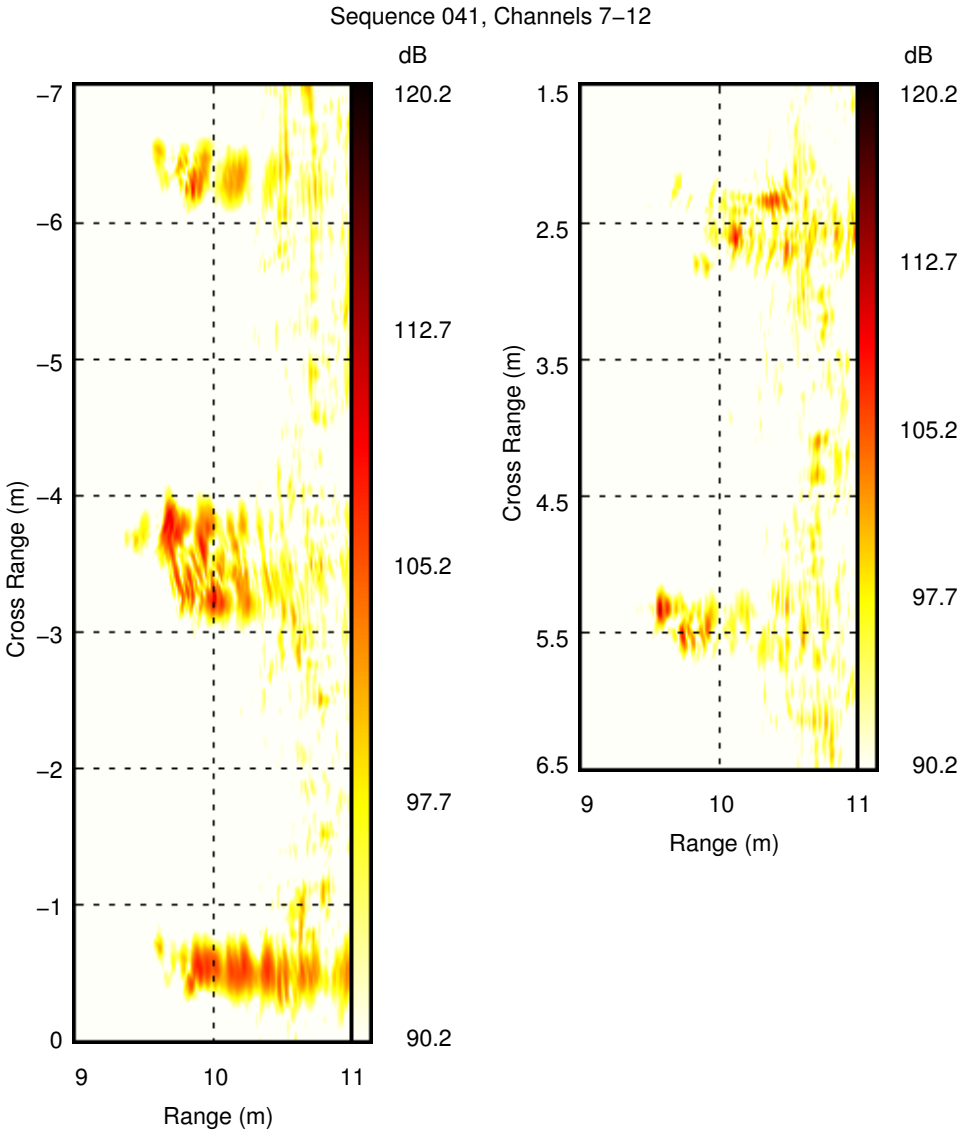

Figure 20: Higher resolution SAS image for sequence 41.

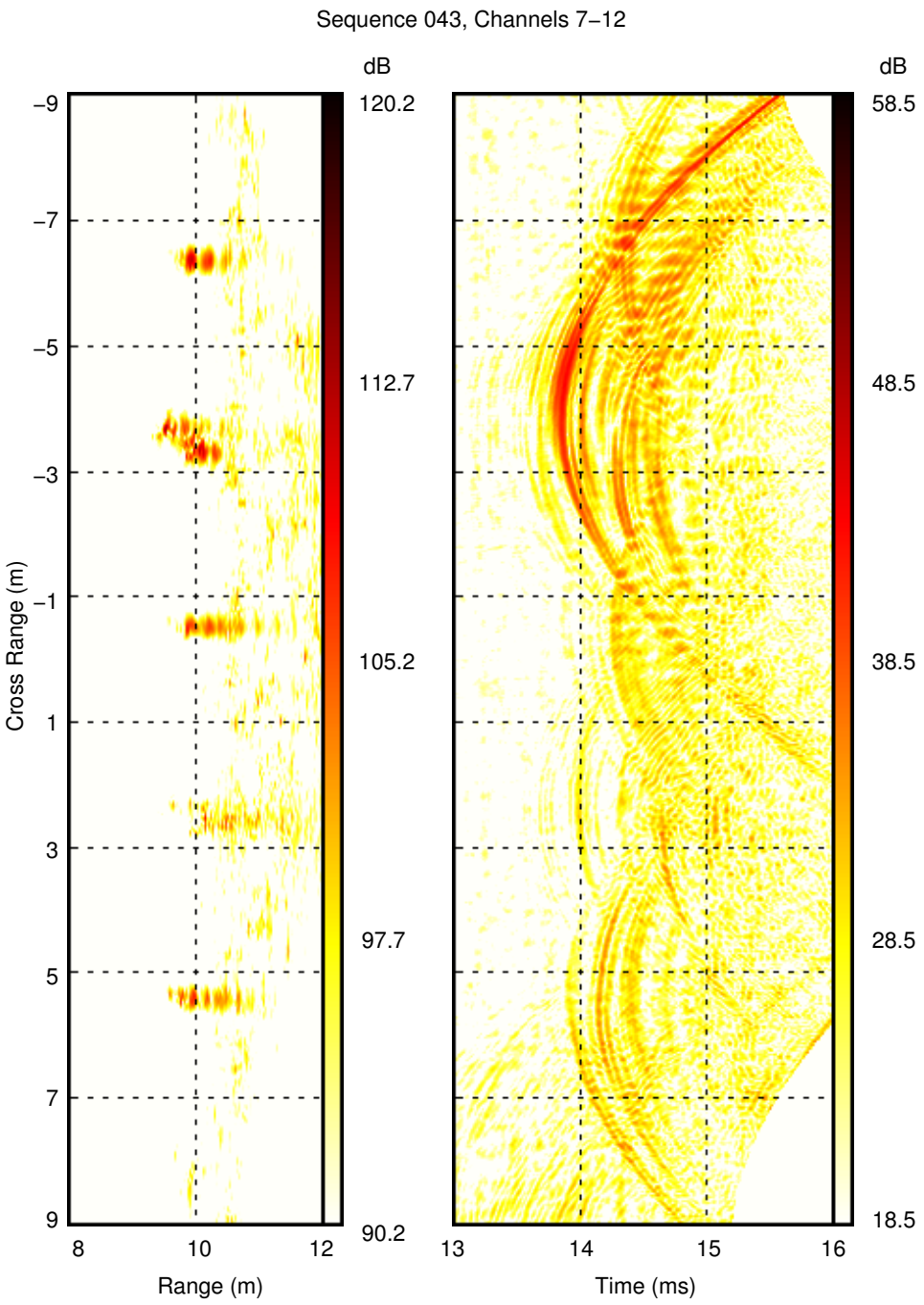

Figure 21: SAS image (left) generated from the pulse-compressed baseband time signals (right) for sequence 43.

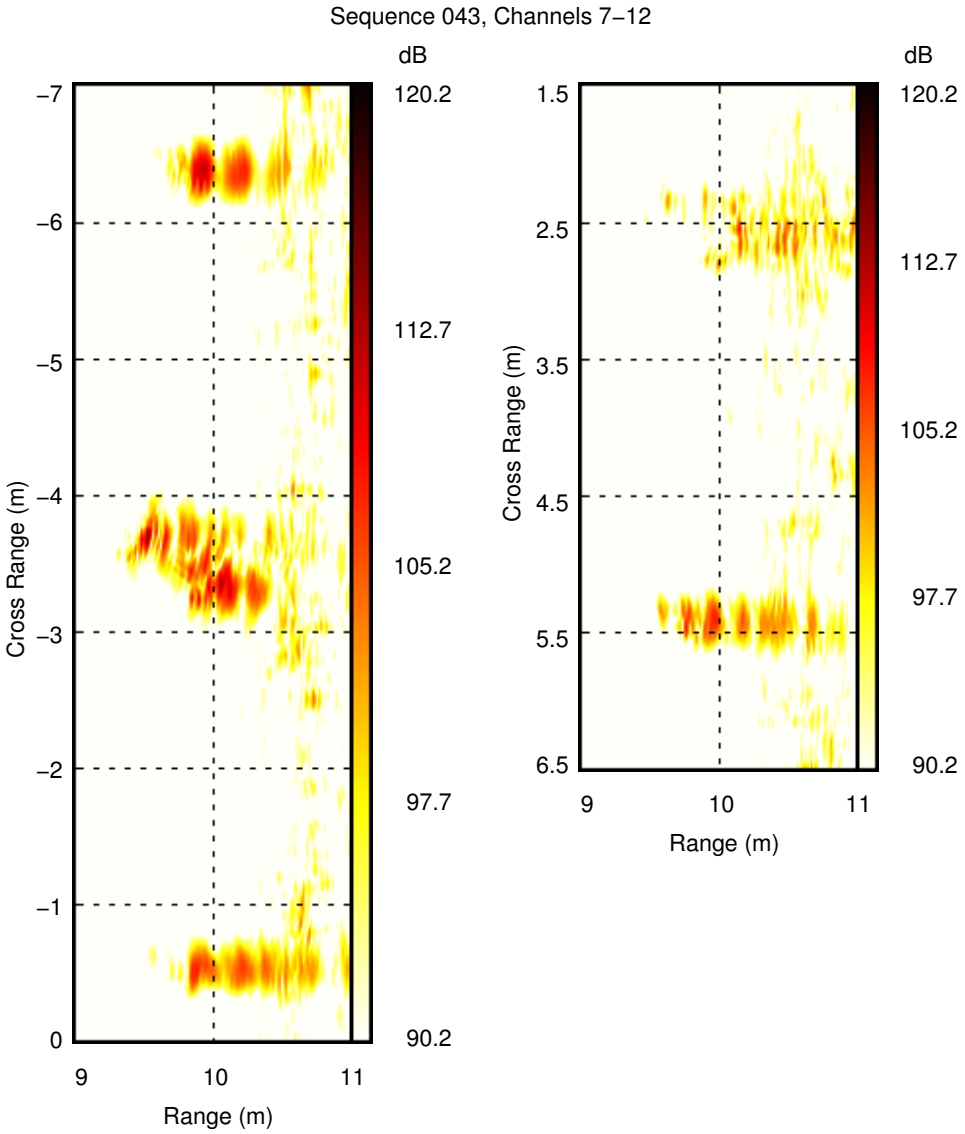

Figure 22: Higher resolution SAS image for sequence 43.

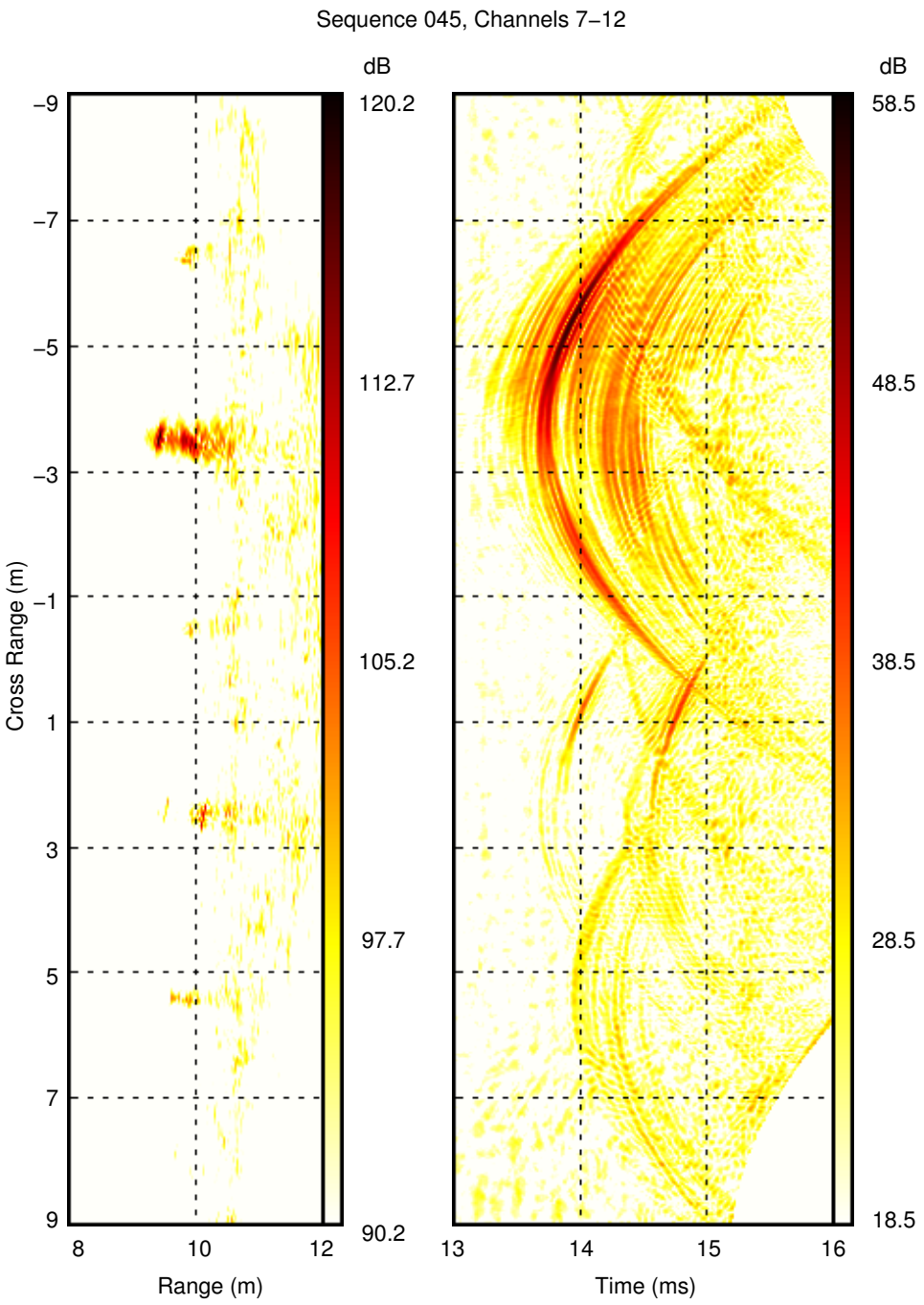

Figure 23: SAS image (left) generated from the pulse-compressed baseband time signals (right) for sequence 45.

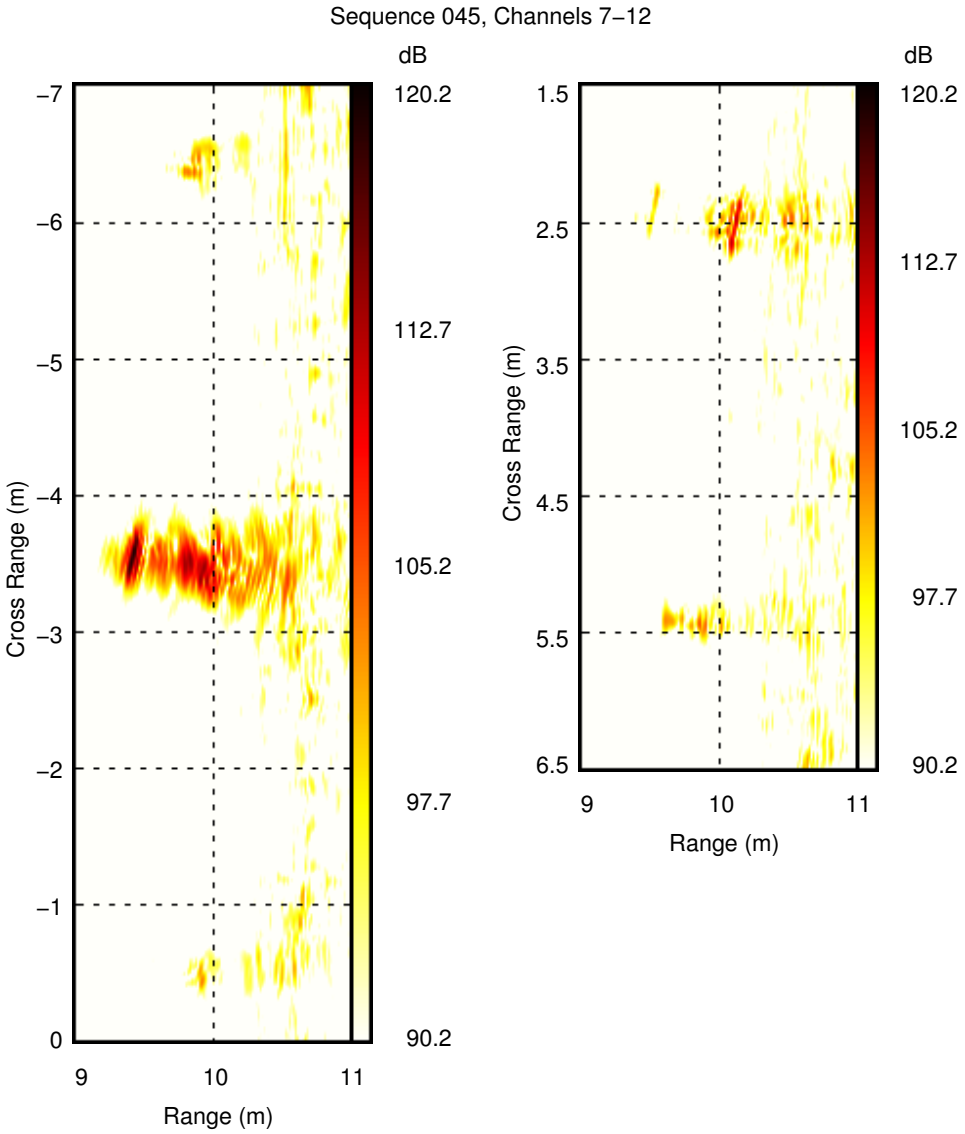

Figure 24: Higher resolution SAS image for sequence 45.

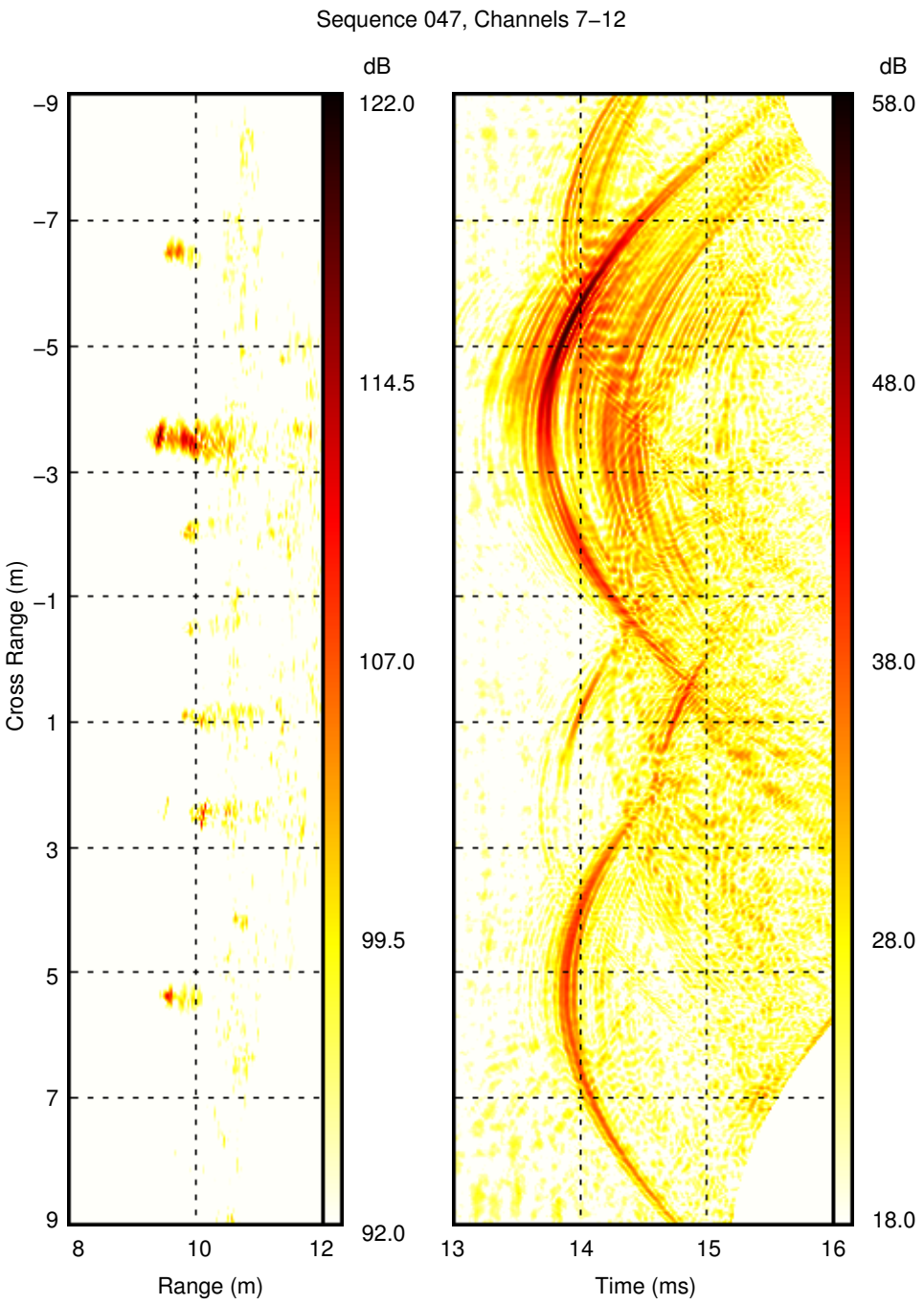

Figure 25: SAS image (left) generated from the pulse-compressed baseband time signals (right) for sequence 47.

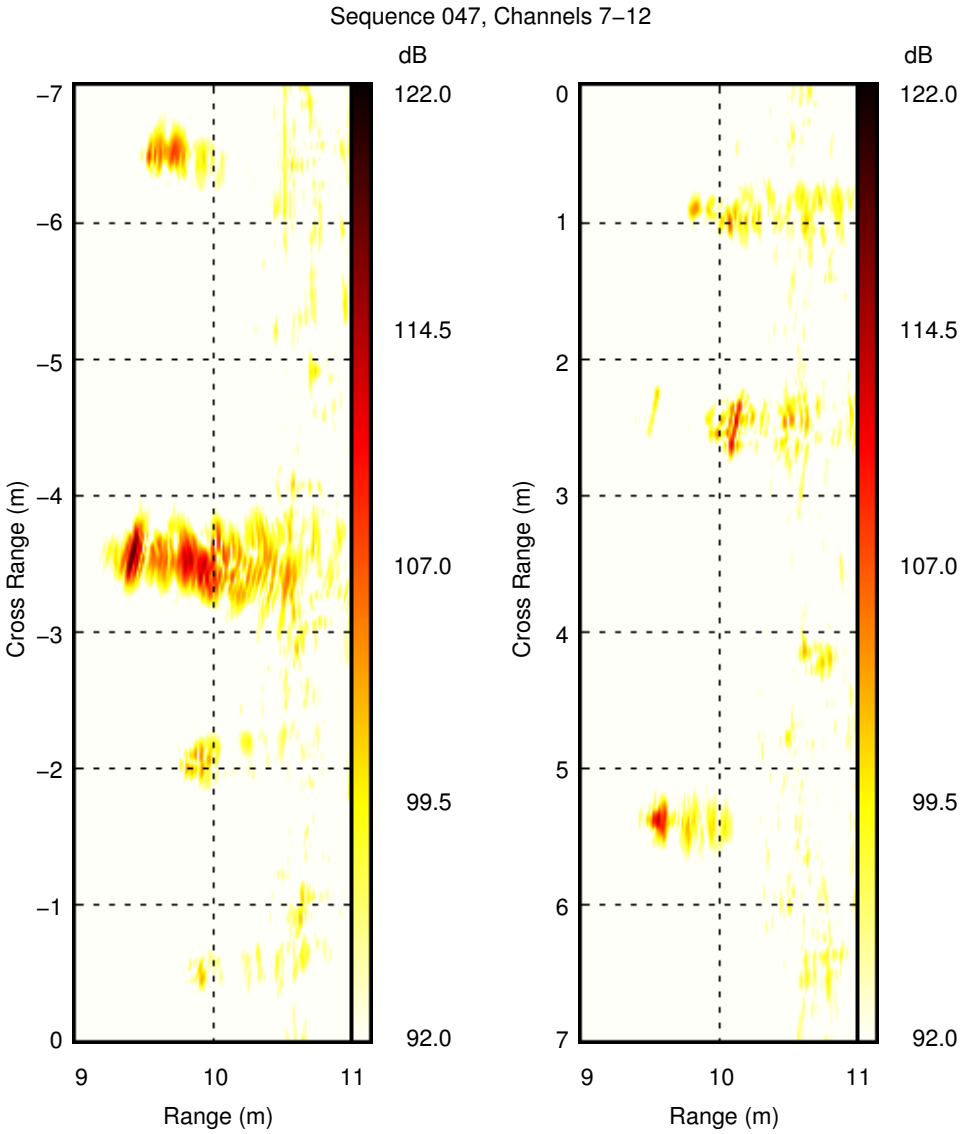

Figure 26: Higher resolution SAS image for sequence 47.

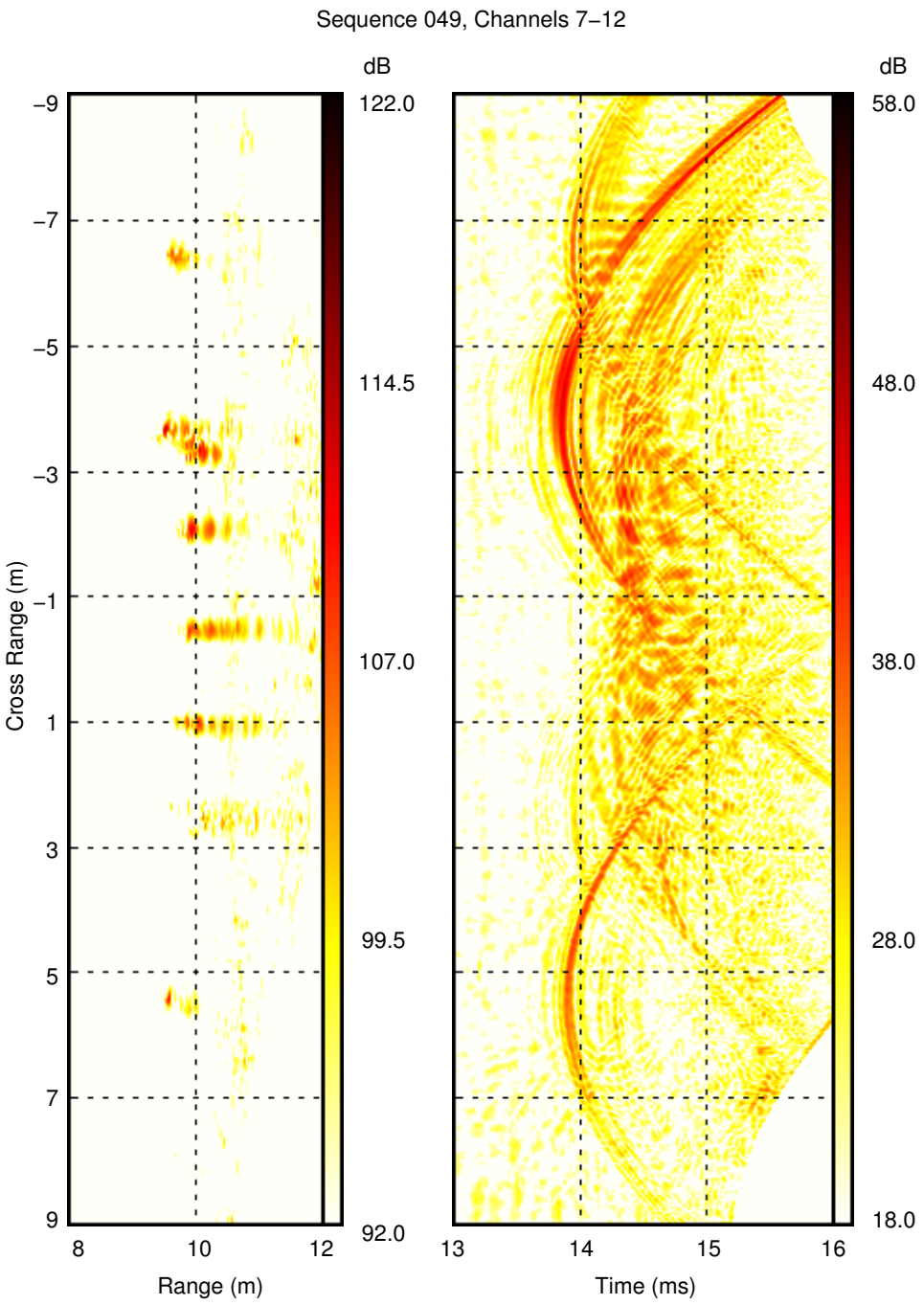

Figure 27: SAS image (left) generated from the pulse-compressed baseband time signals (right) for sequence 49.

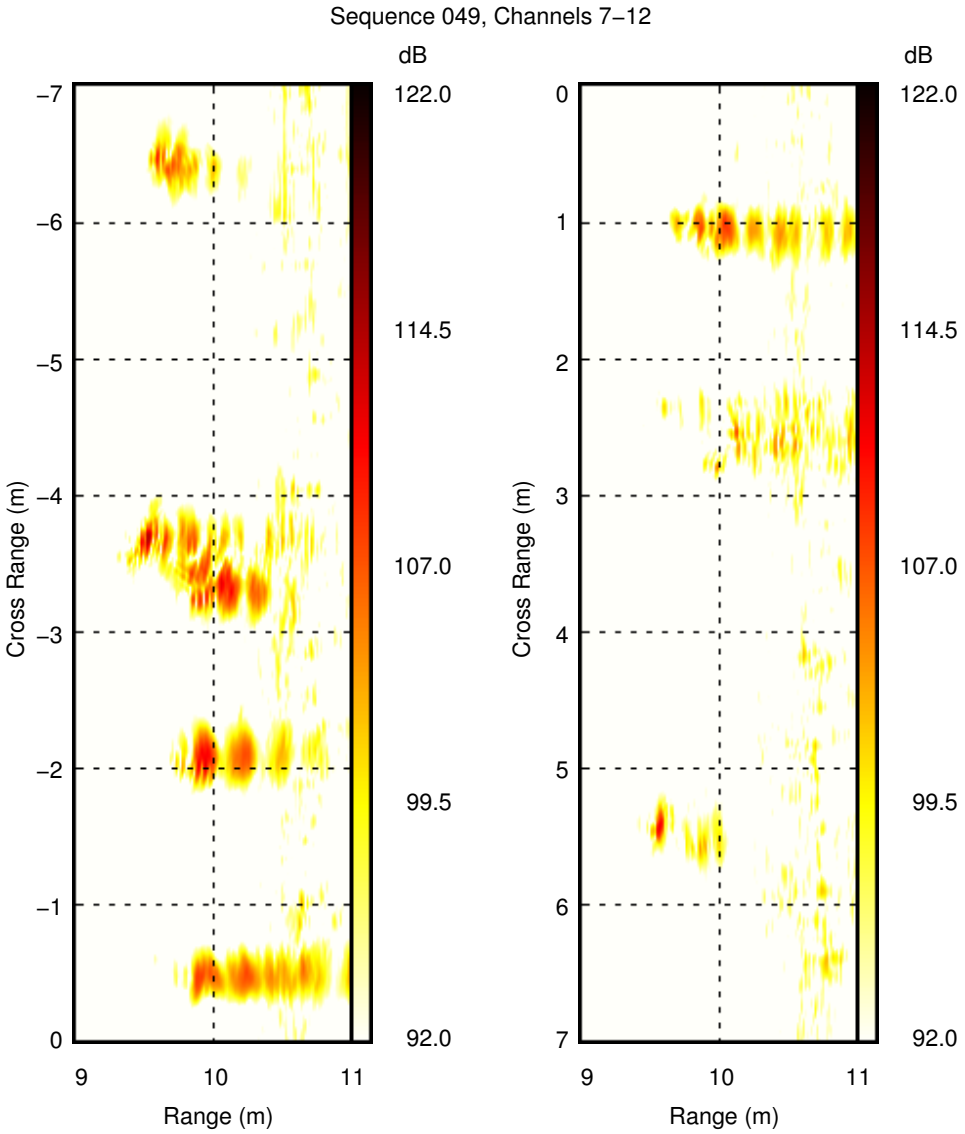

Figure 28: Higher resolution SAS image for sequence 49.

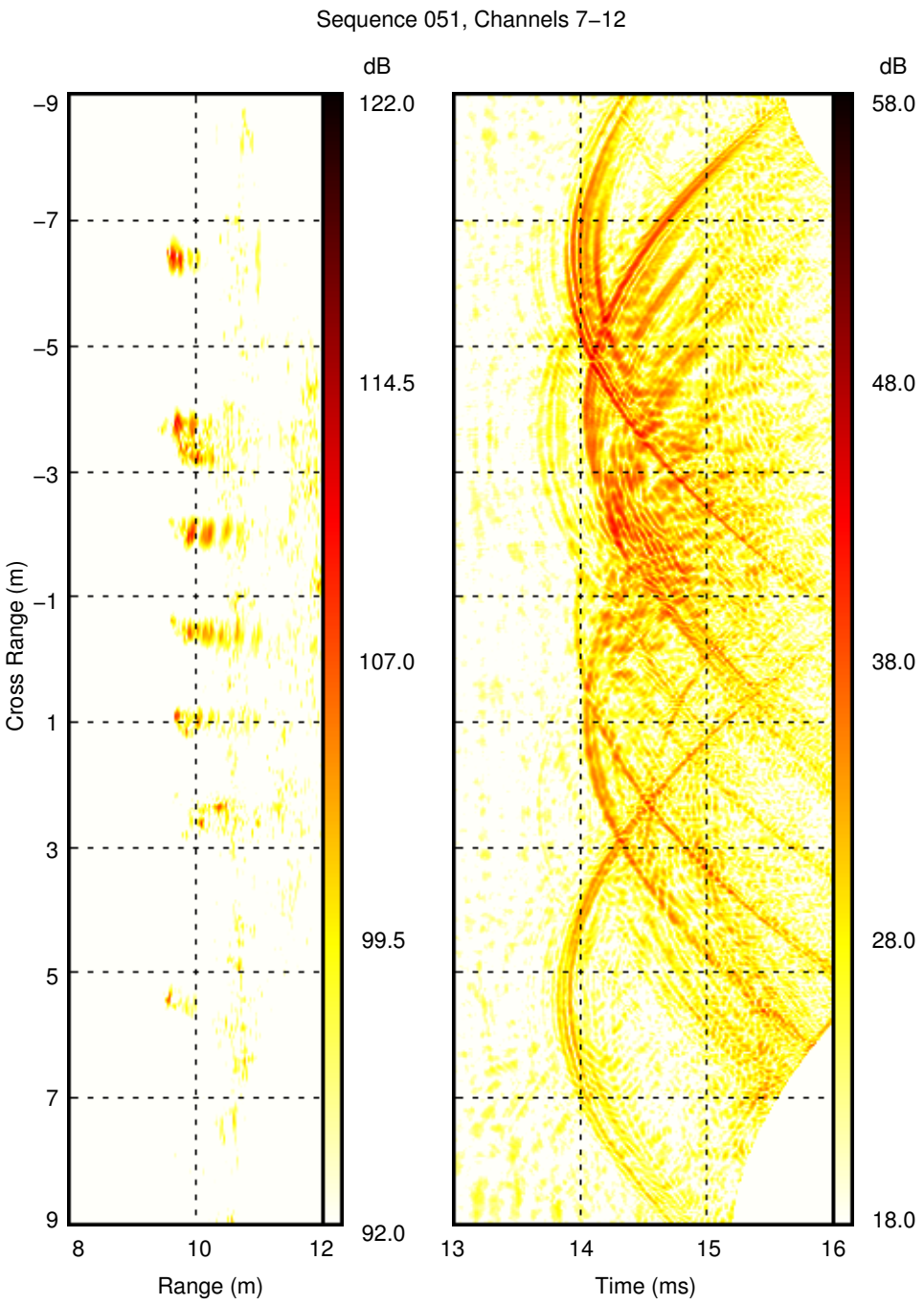

Figure 29: SAS image (left) generated from the pulse-compressed baseband time signals (right) for sequence 51.

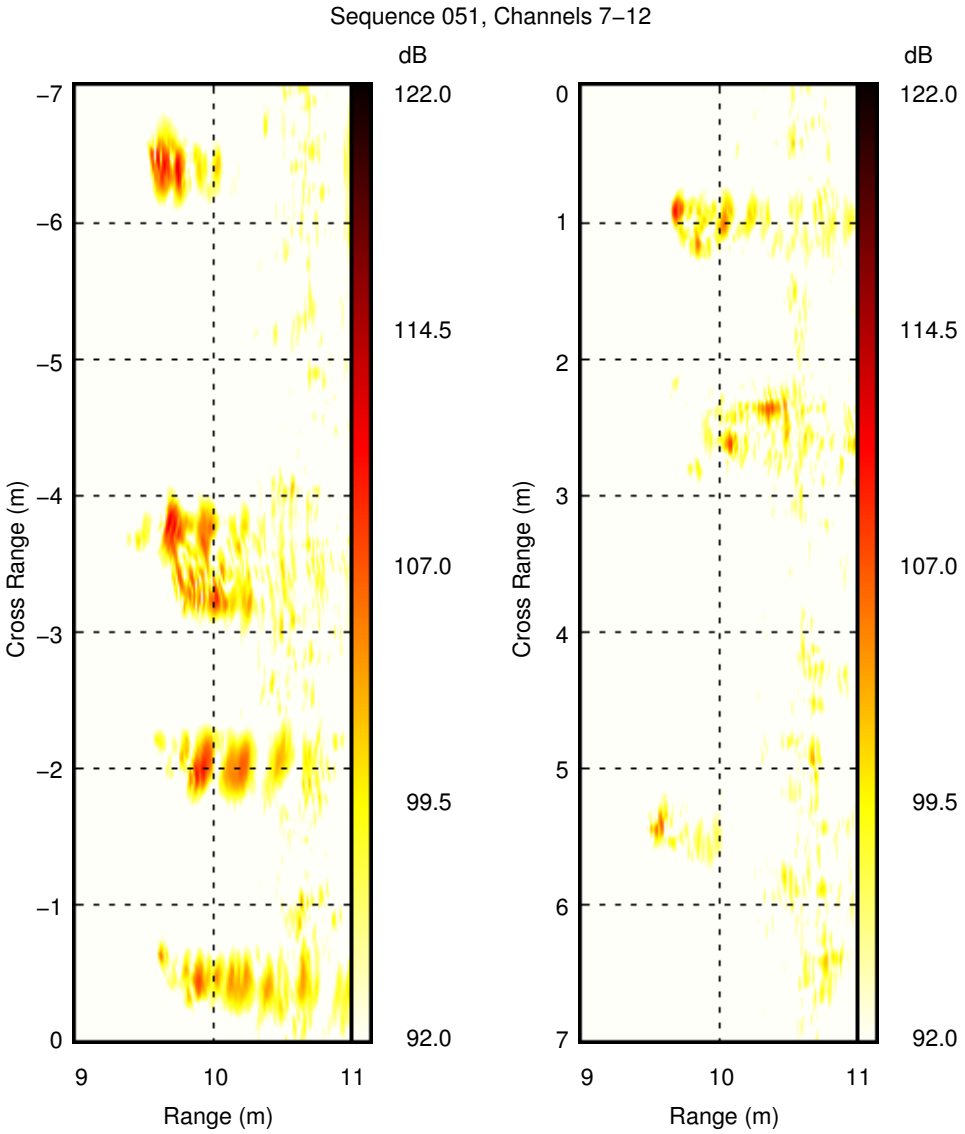

Figure 30: Higher resolution SAS image for sequence 51.

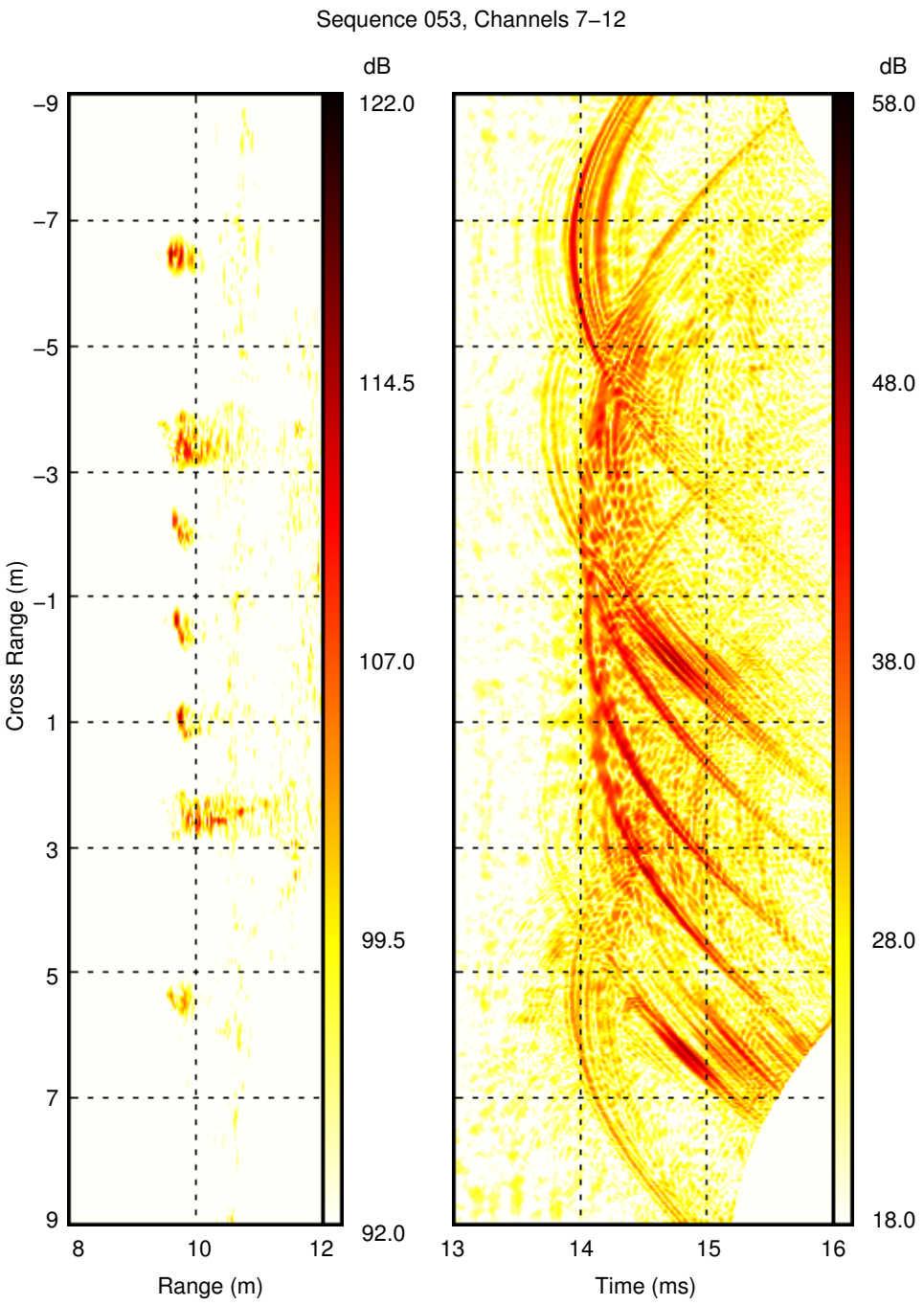

Figure 31: SAS image (left) generated from the pulse-compressed baseband time signals (right) for sequence 53.

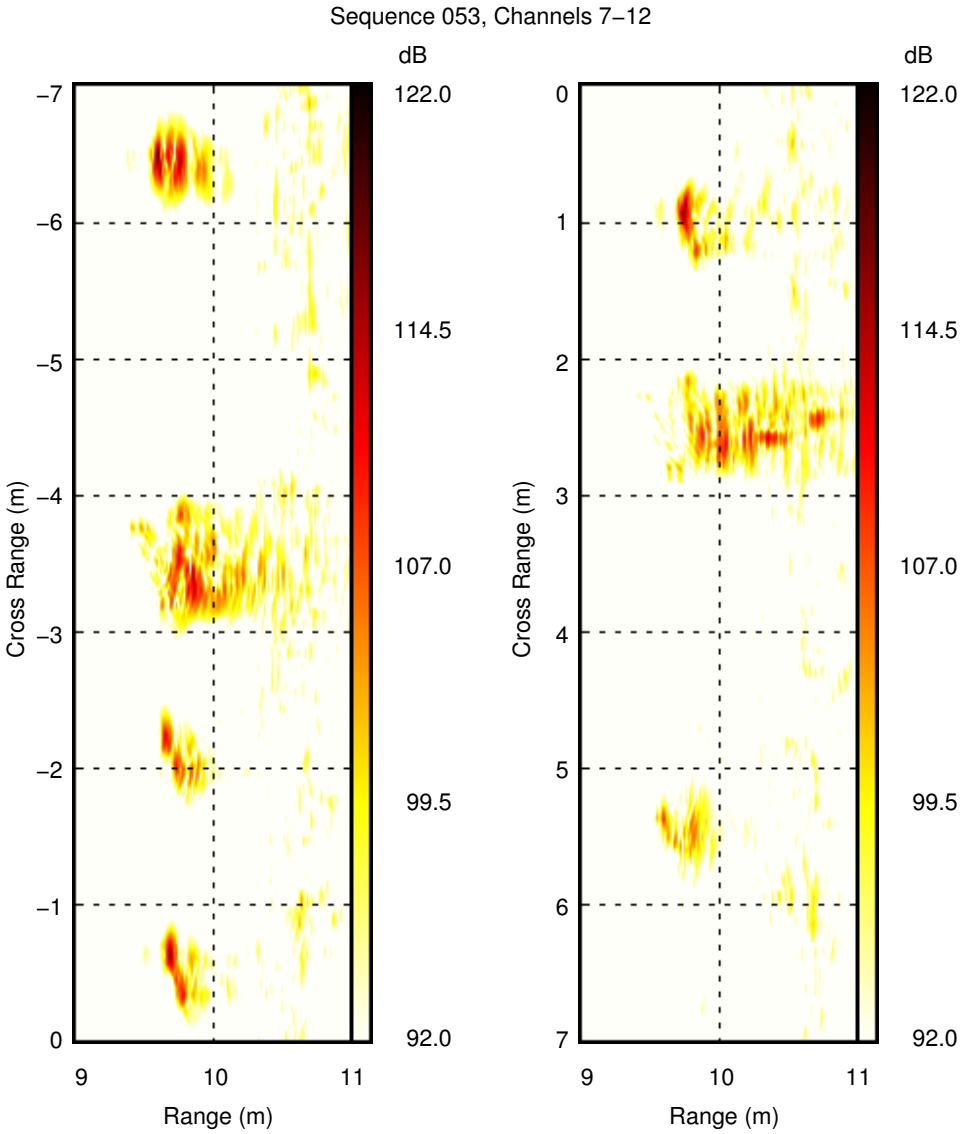

Figure 32: Higher resolution SAS image for sequence 53.

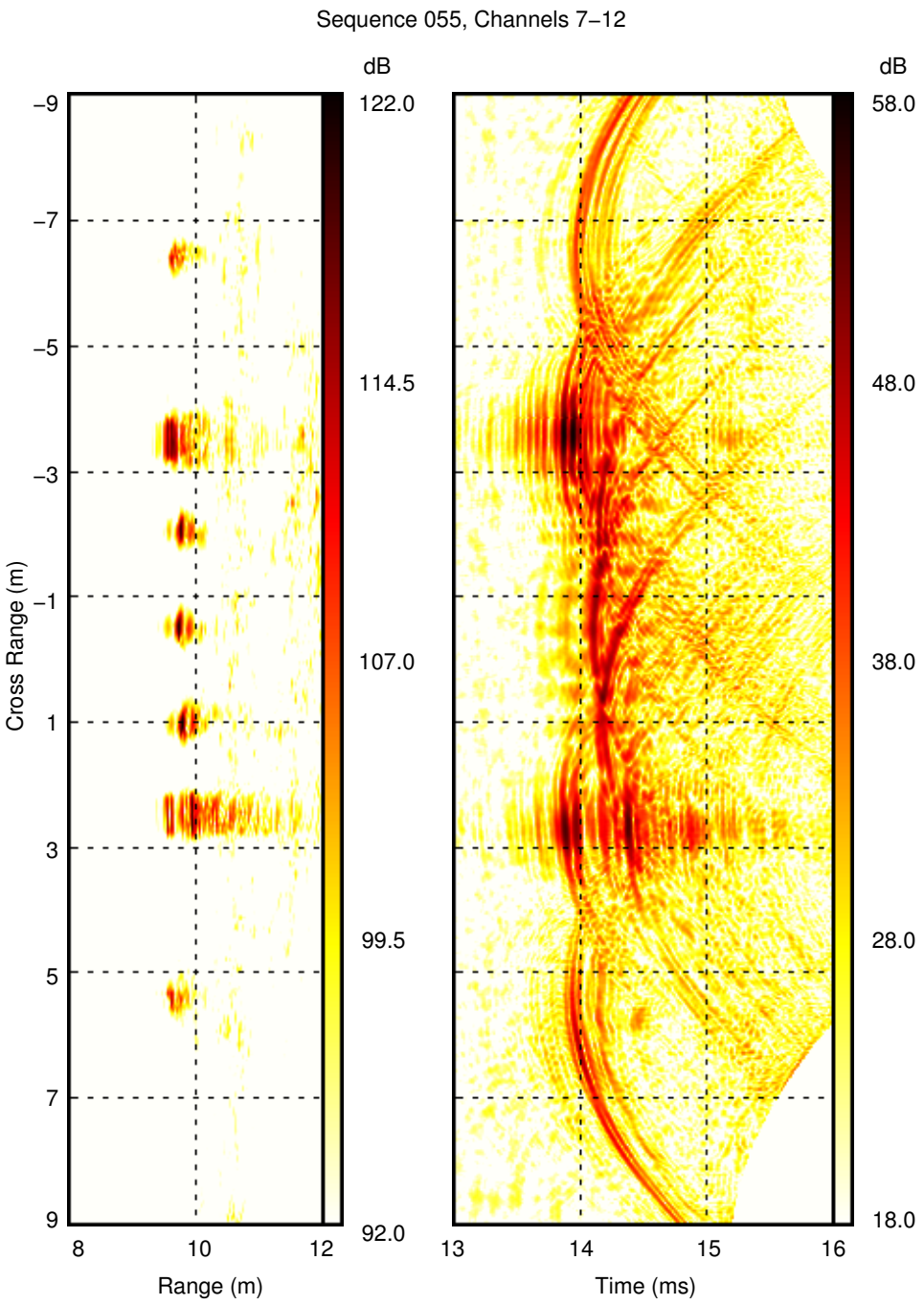

Figure 33: SAS image (left) generated from the pulse-compressed baseband time signals (right) for sequence 55.

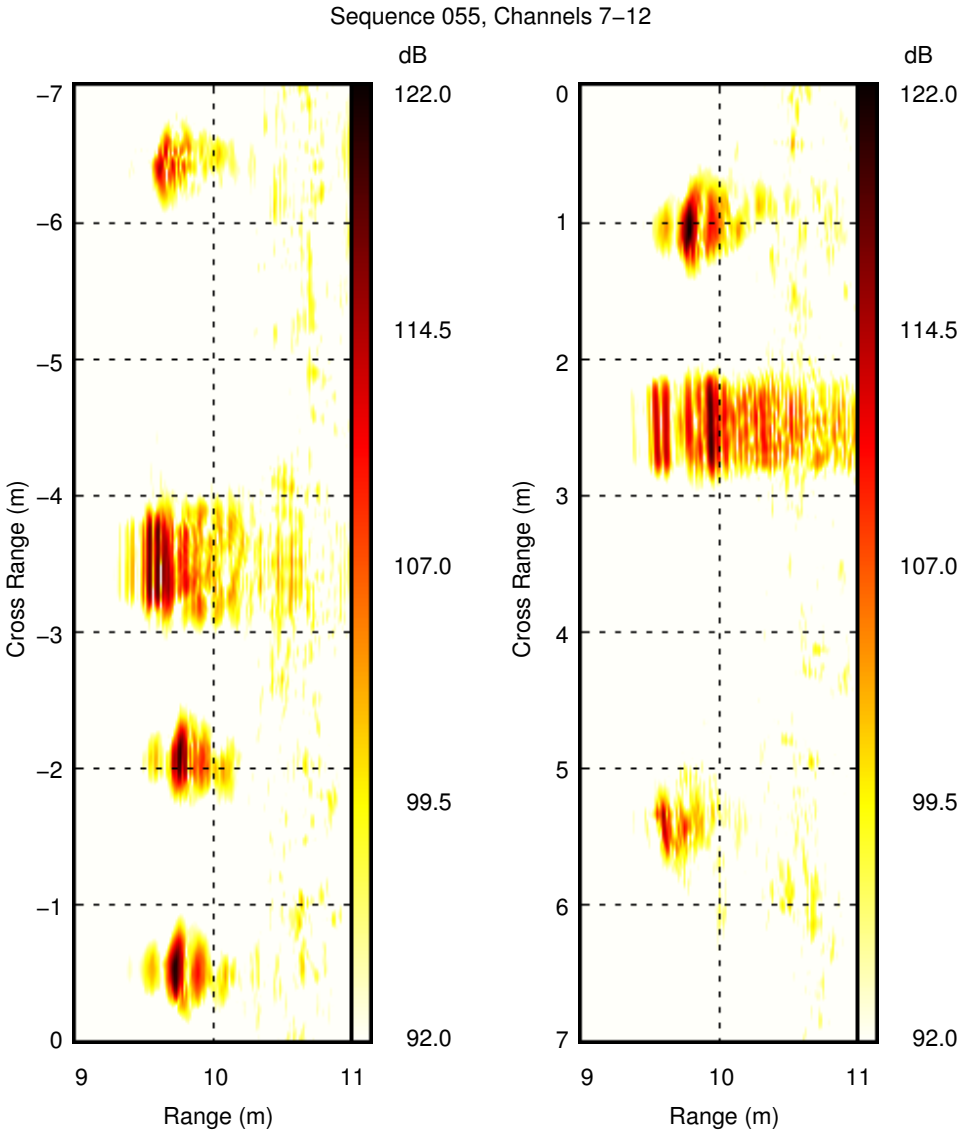

Figure 34: Higher resolution SAS image for sequence 55.

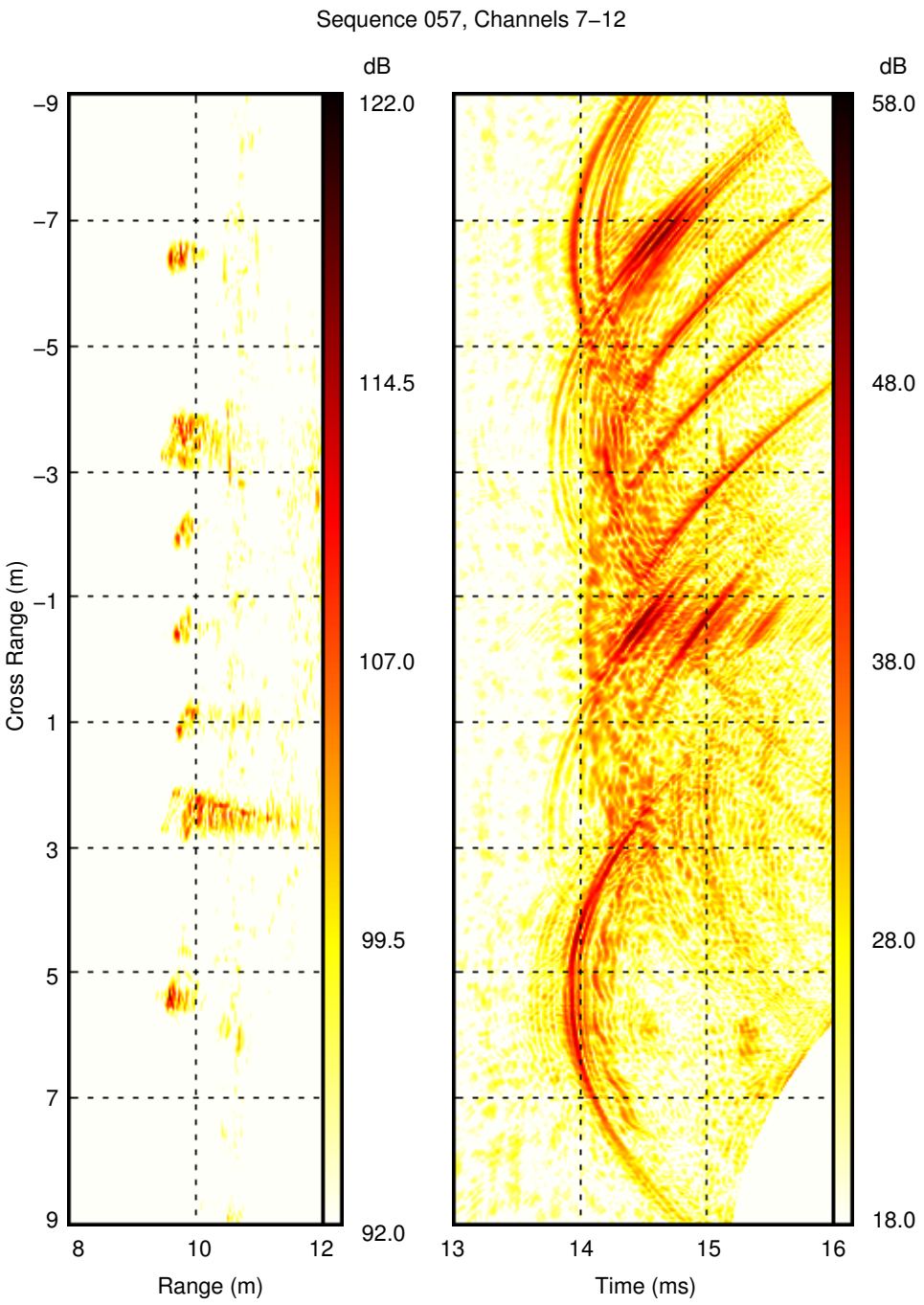

Figure 35: SAS image (left) generated from the pulse-compressed baseband time signals (right) for sequence 57.

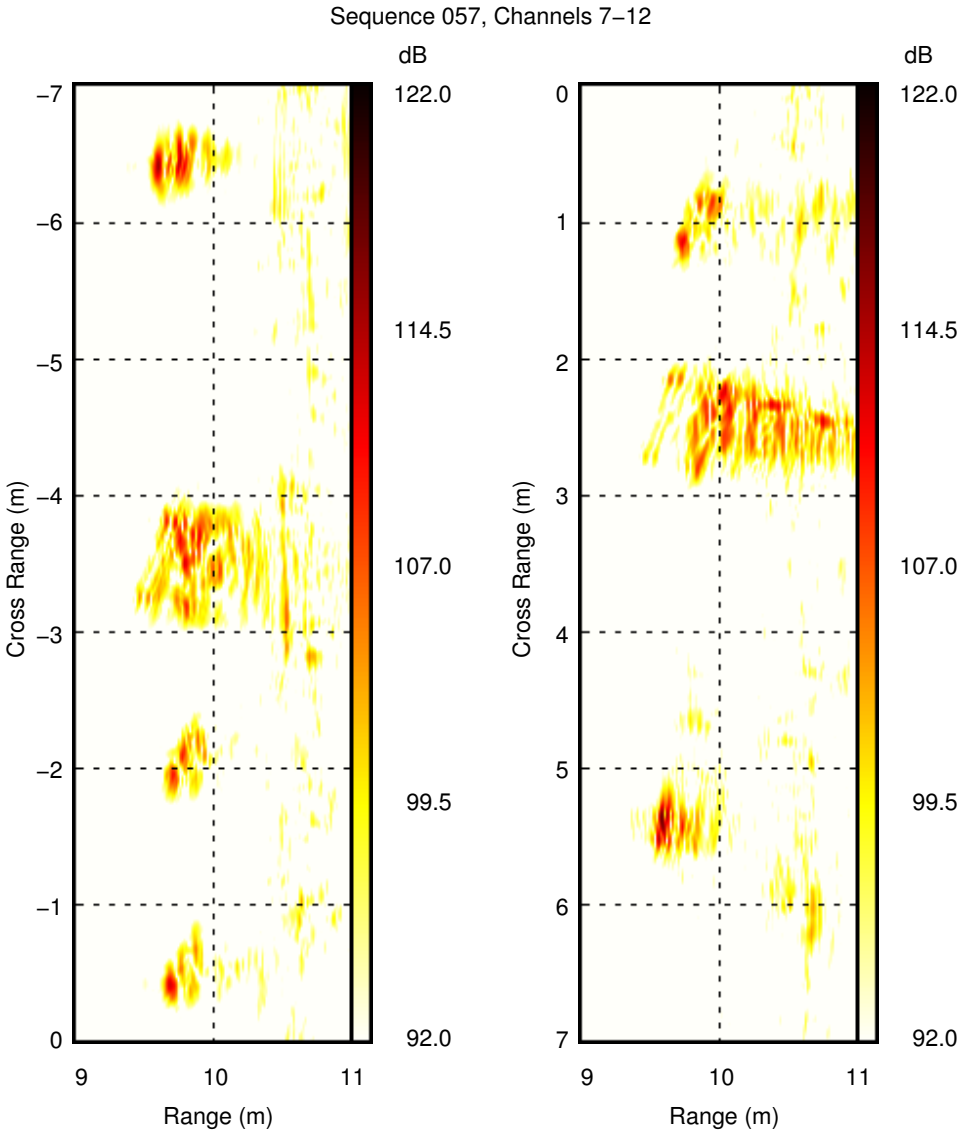

Figure 36: Higher resolution SAS image for sequence 57.

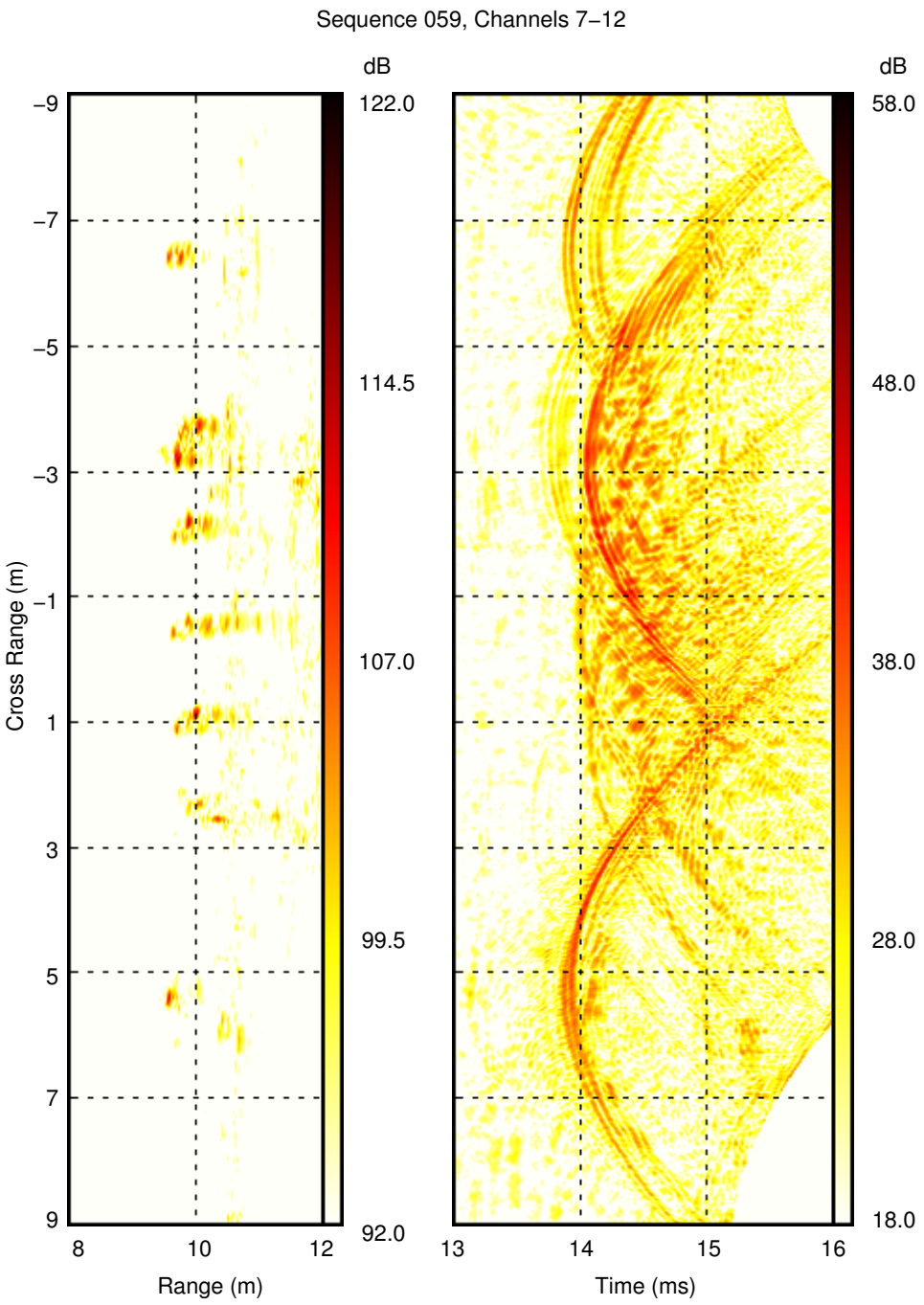

Figure 37: SAS image (left) generated from the pulse-compressed baseband time signals (right) for sequence 59.

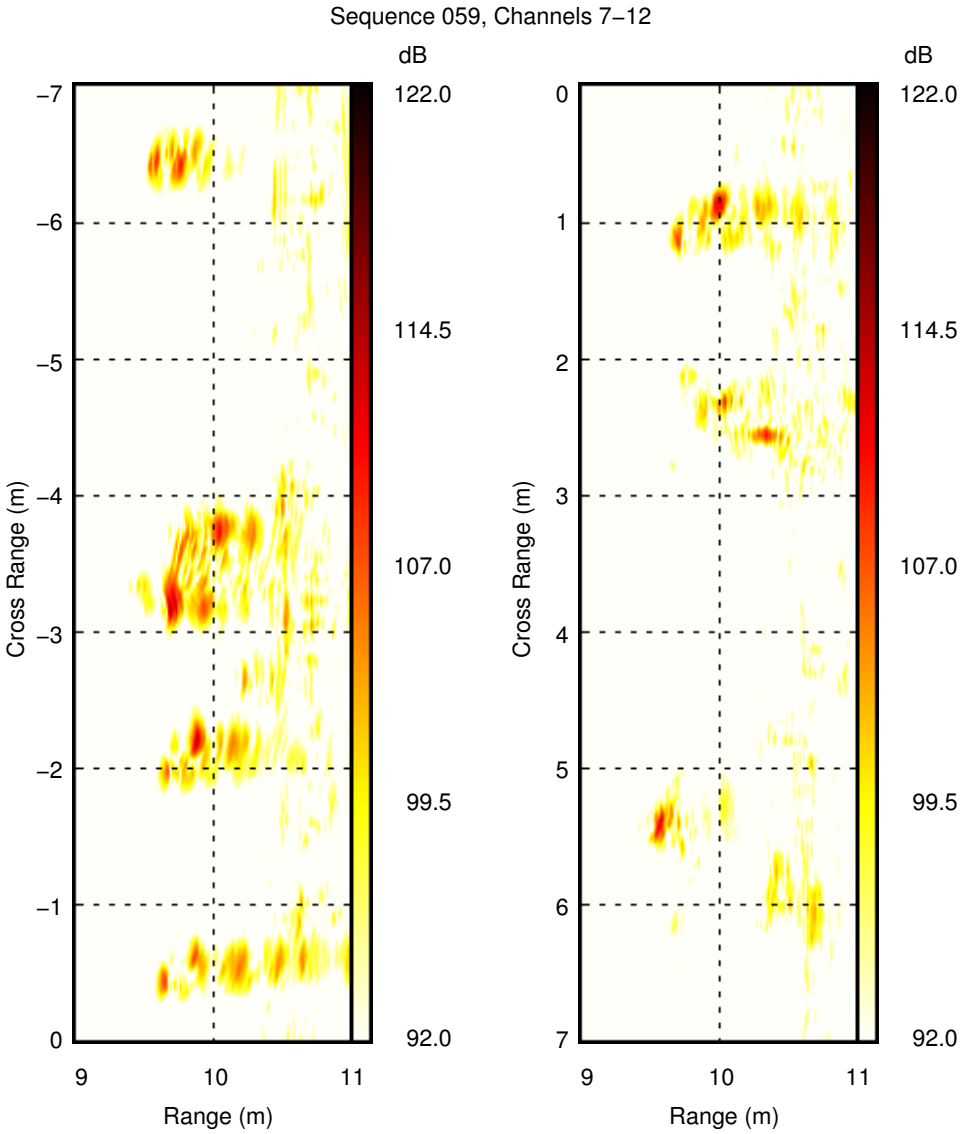

Figure 38: Higher resolution SAS image for sequence 59.

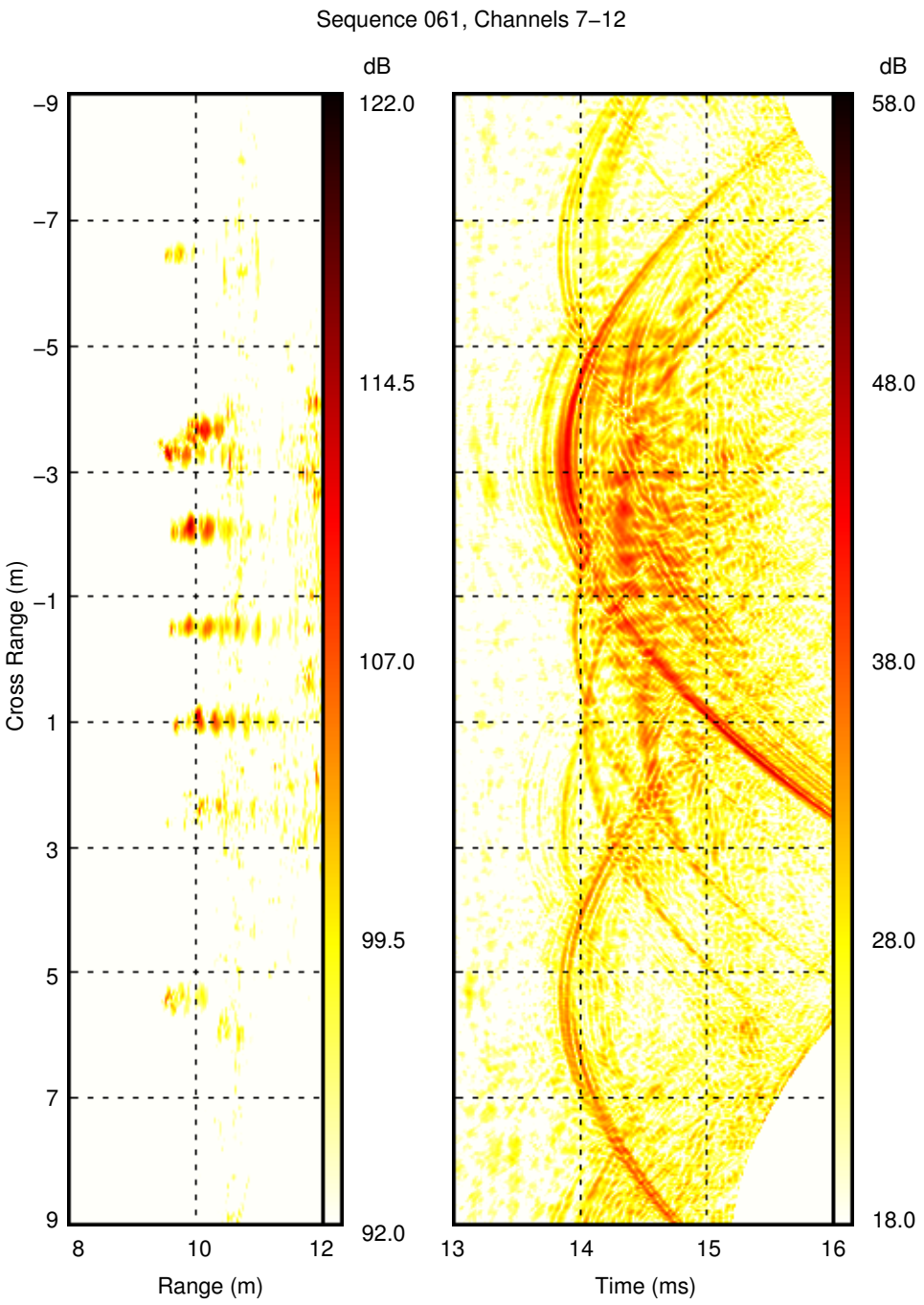

Figure 39: SAS image (left) generated from the pulse-compressed baseband time signals (right) for sequence 61.

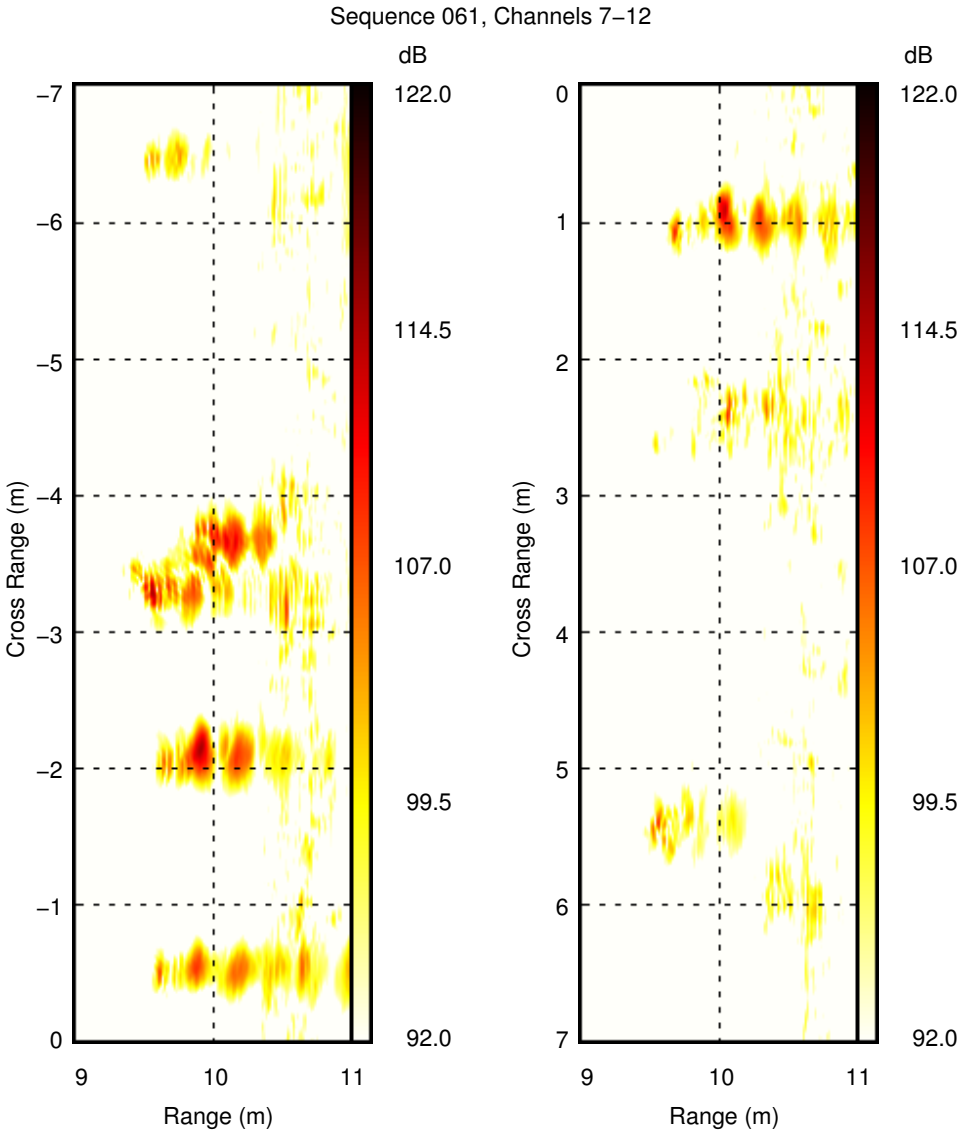

Figure 40: Higher resolution SAS image for sequence 61.

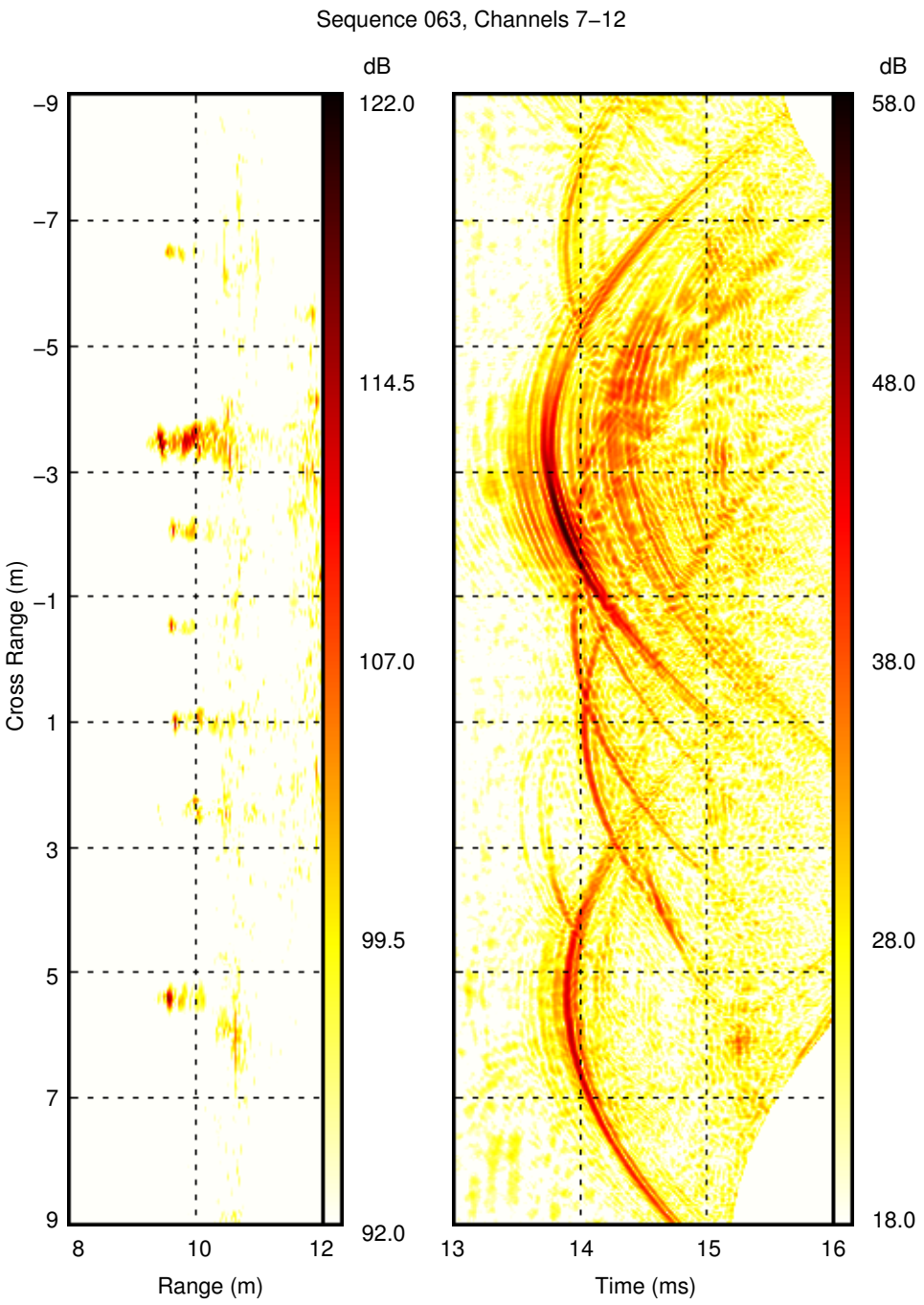

Figure 41: SAS image (left) generated from the pulse-compressed baseband time signals (right) for sequence 63.

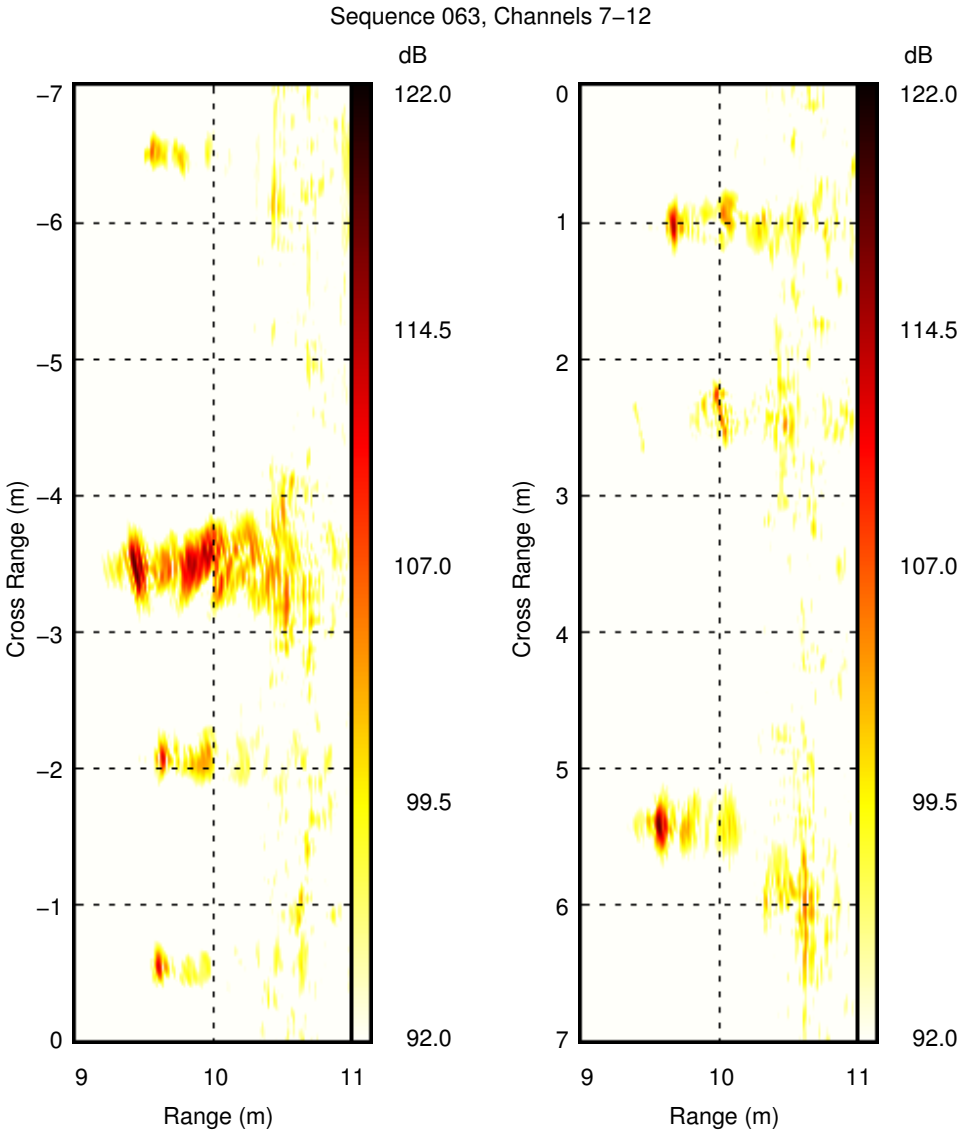

Figure 42: Higher resolution SAS image for sequence 63.

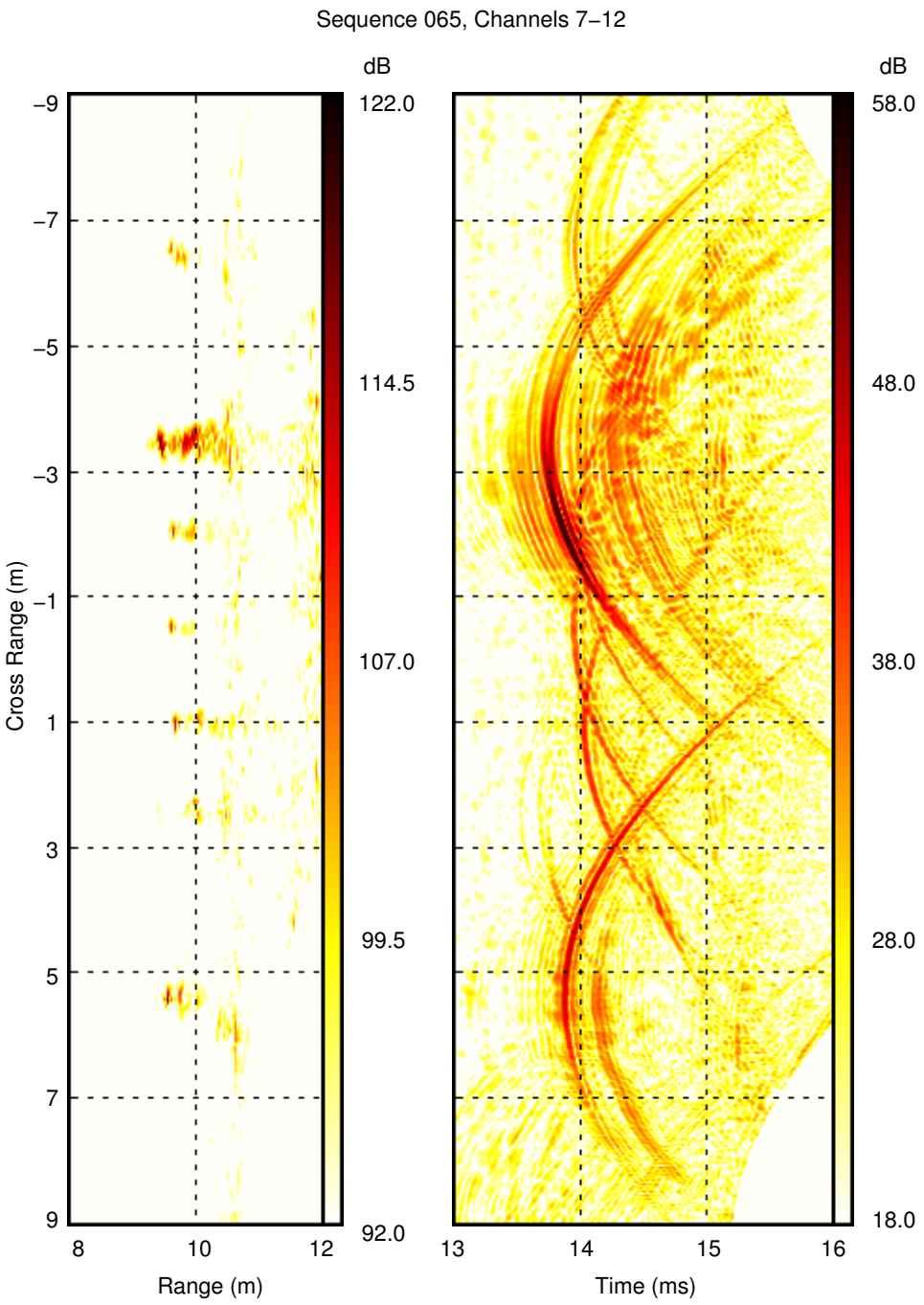

Figure 43: SAS image (left) generated from the pulse-compressed baseband time signals (right) for sequence 65.

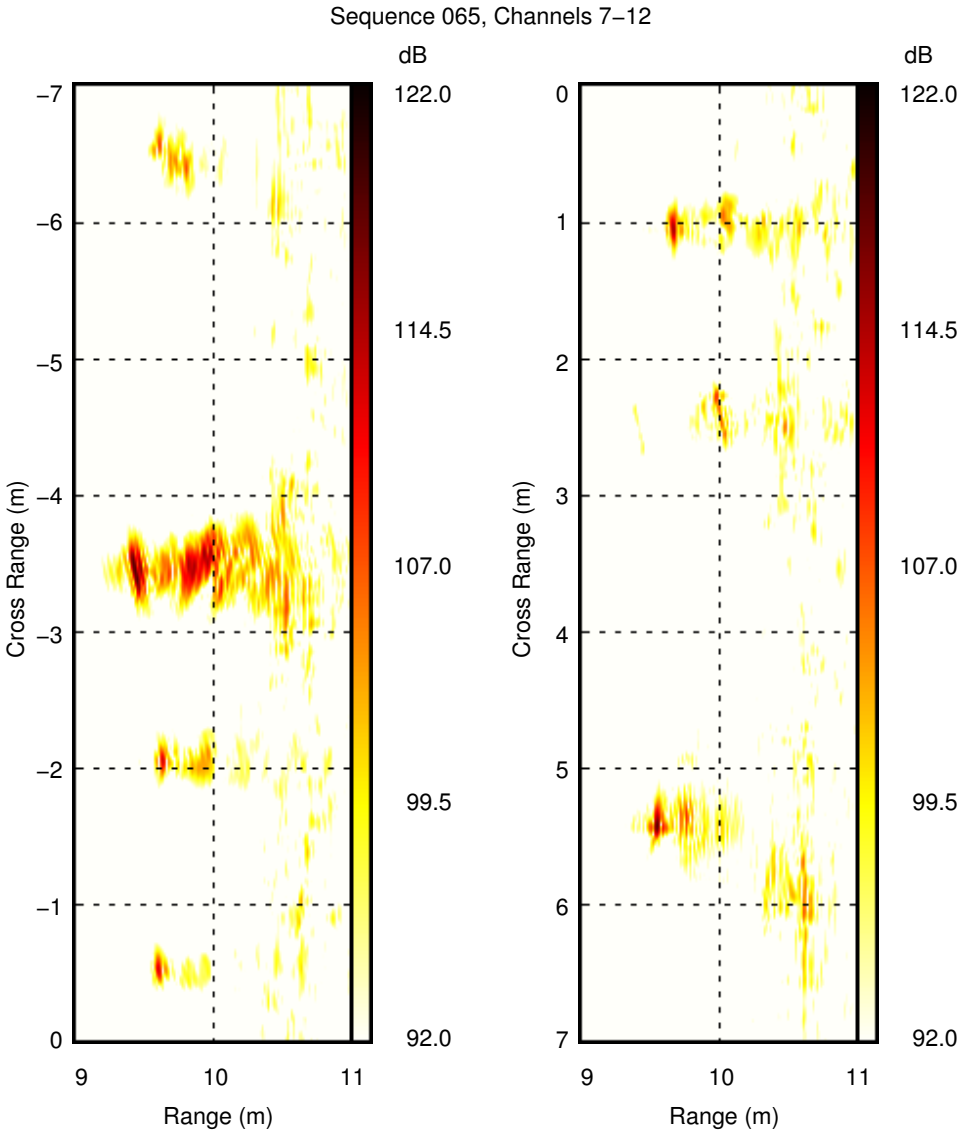

Figure 44: Higher resolution SAS image for sequence 65.

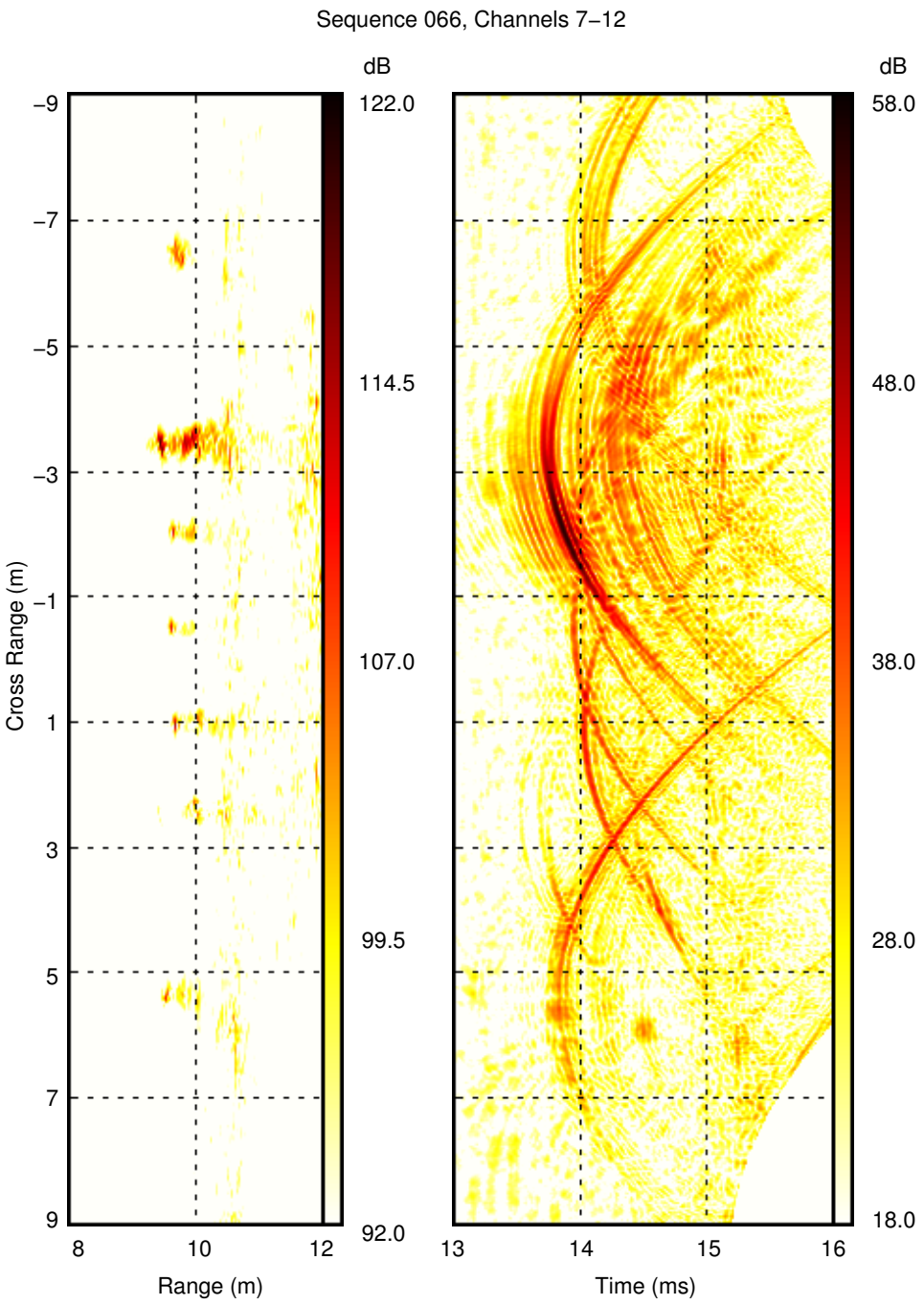

Figure 45: SAS image (left) generated from the pulse-compressed baseband time signals (right) for sequence 66.

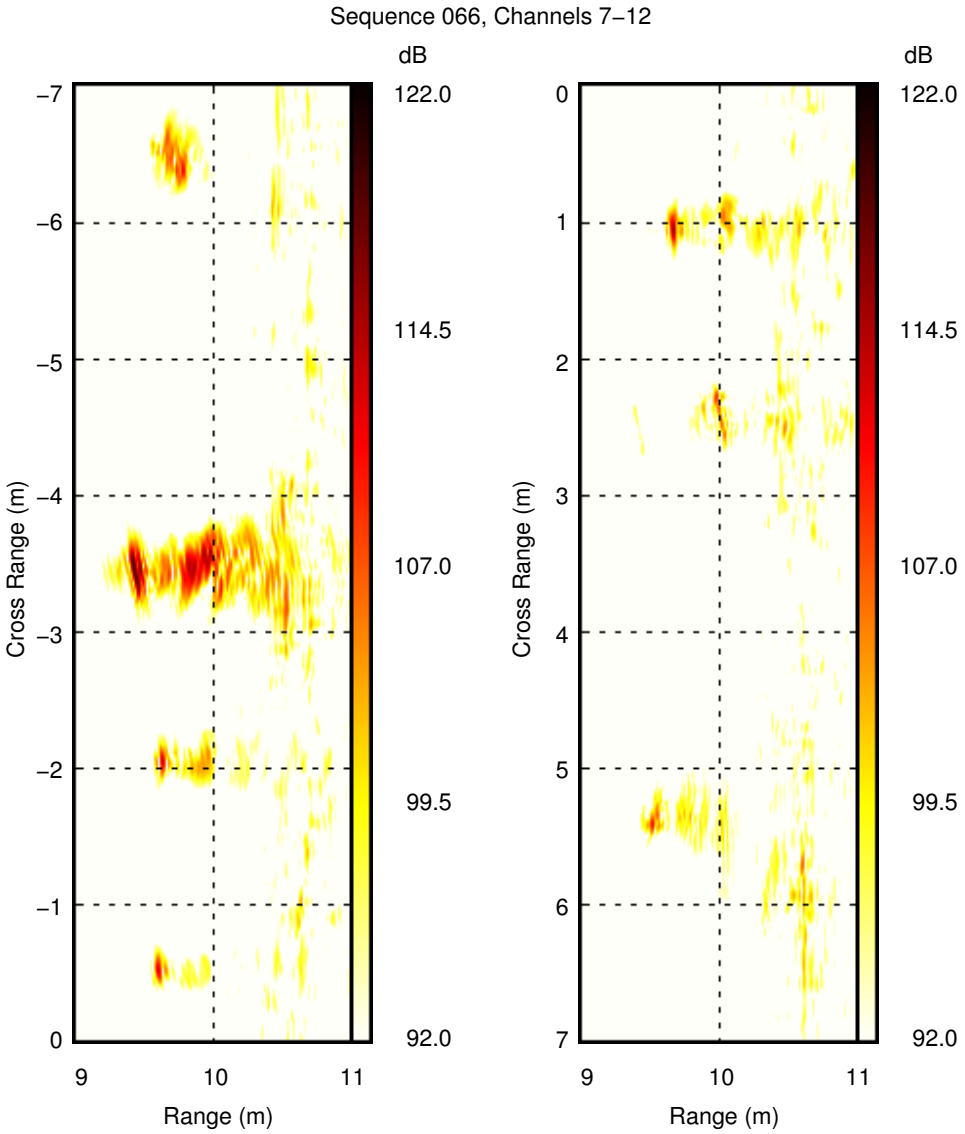

Figure 46: Higher resolution SAS image for sequence 66.

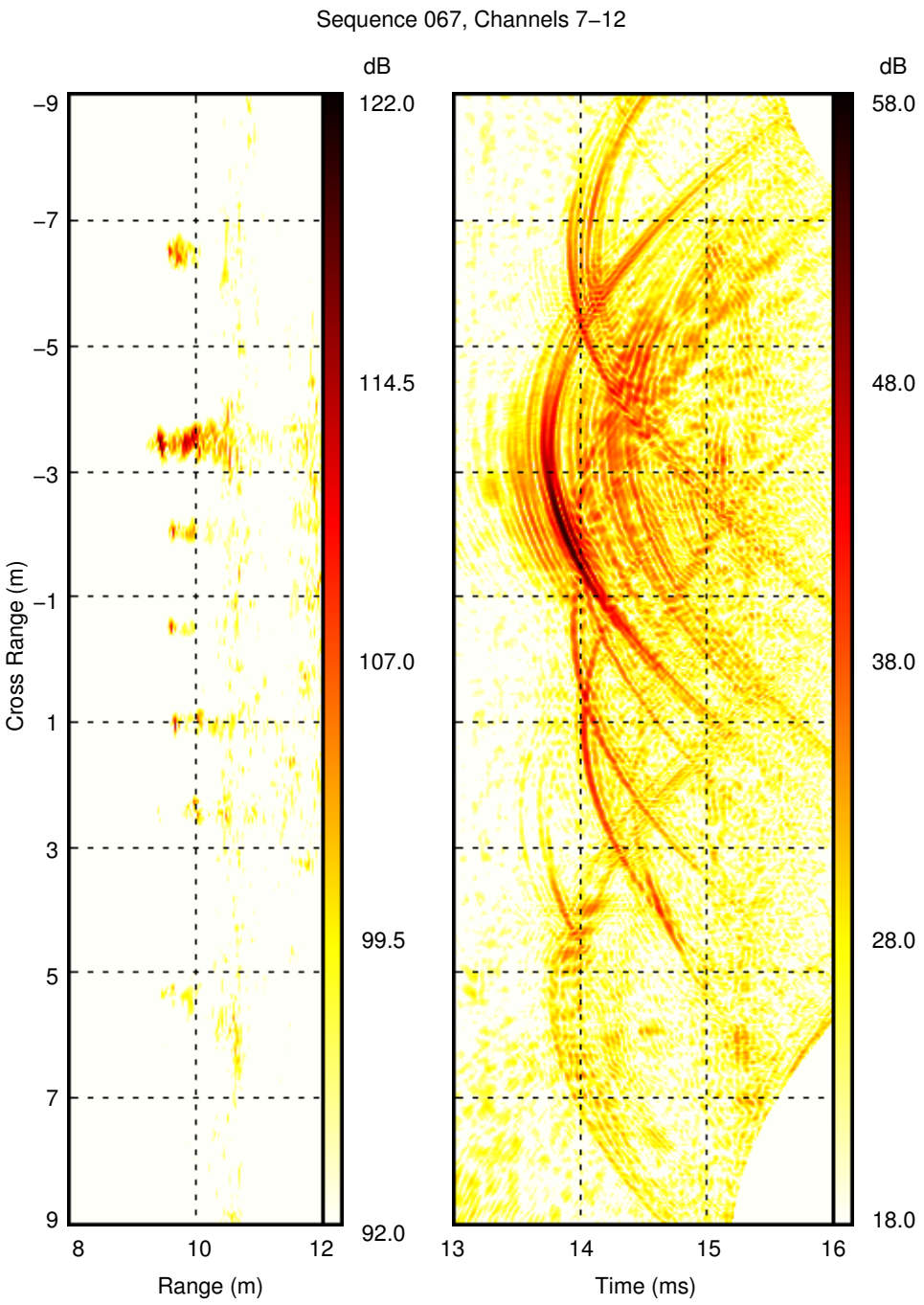

Figure 47: SAS image (left) generated from the pulse-compressed baseband time signals (right) for sequence 67.

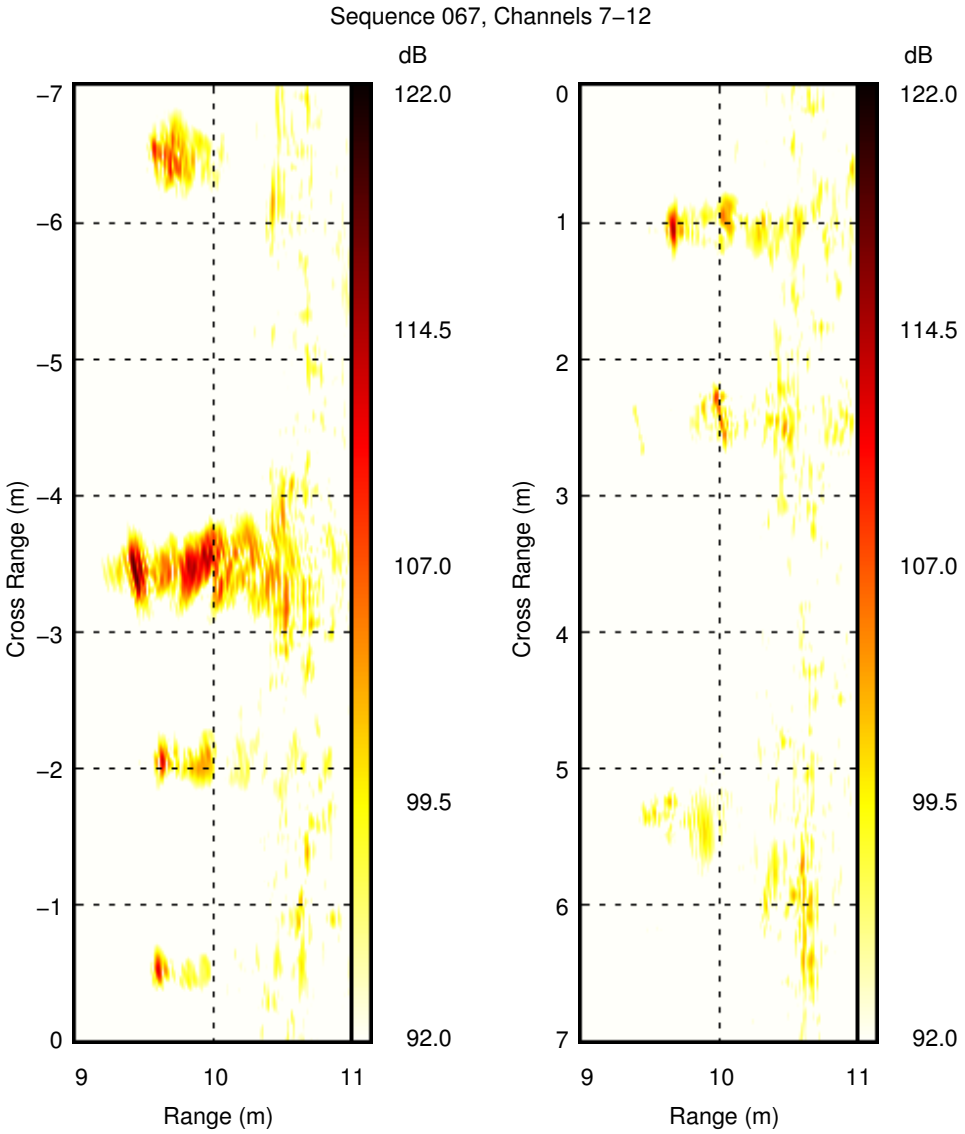

Figure 48: Higher resolution SAS image for sequence 67.

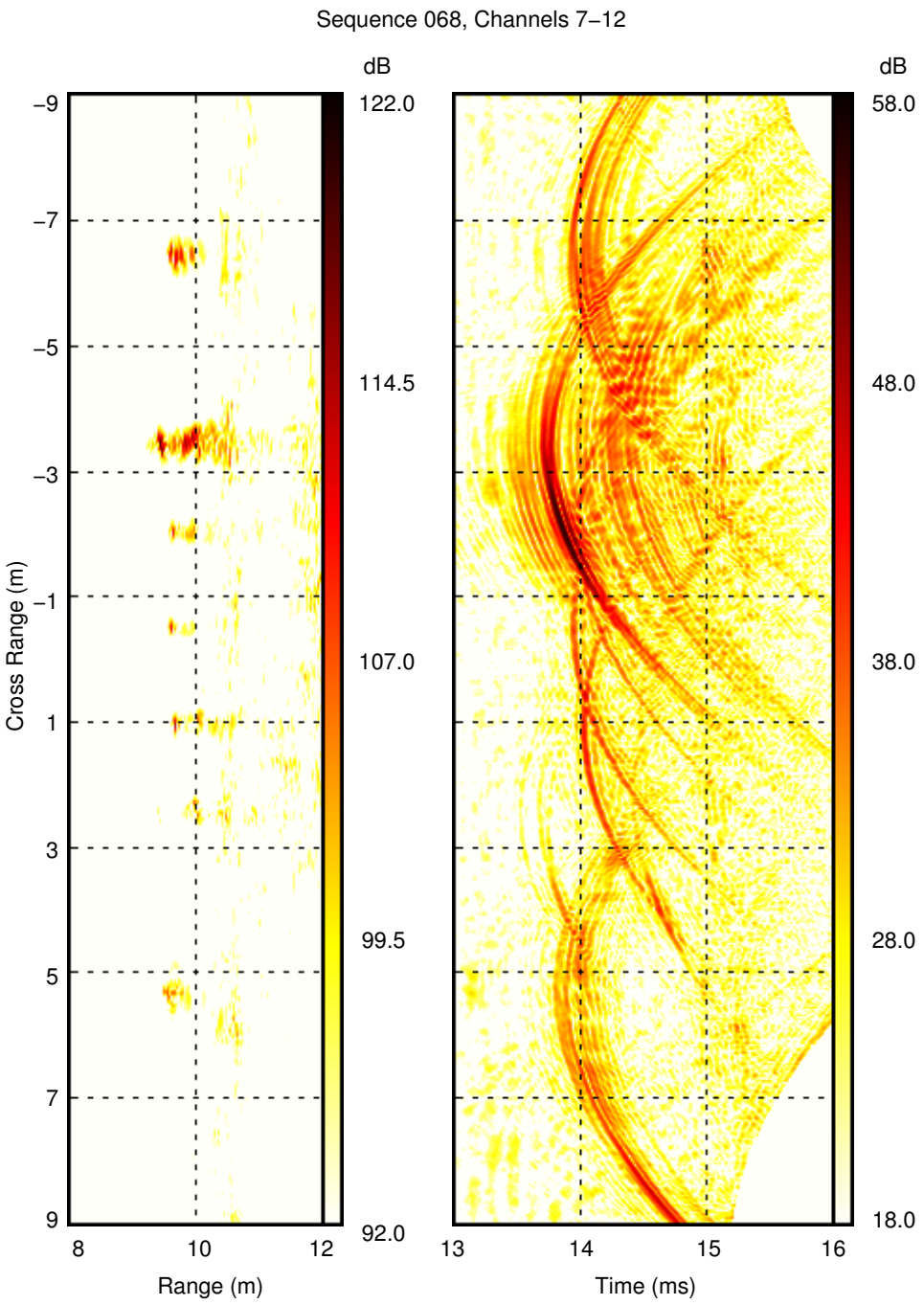

Figure 49: SAS image (left) generated from the pulse-compressed baseband time signals (right) for sequence 68.

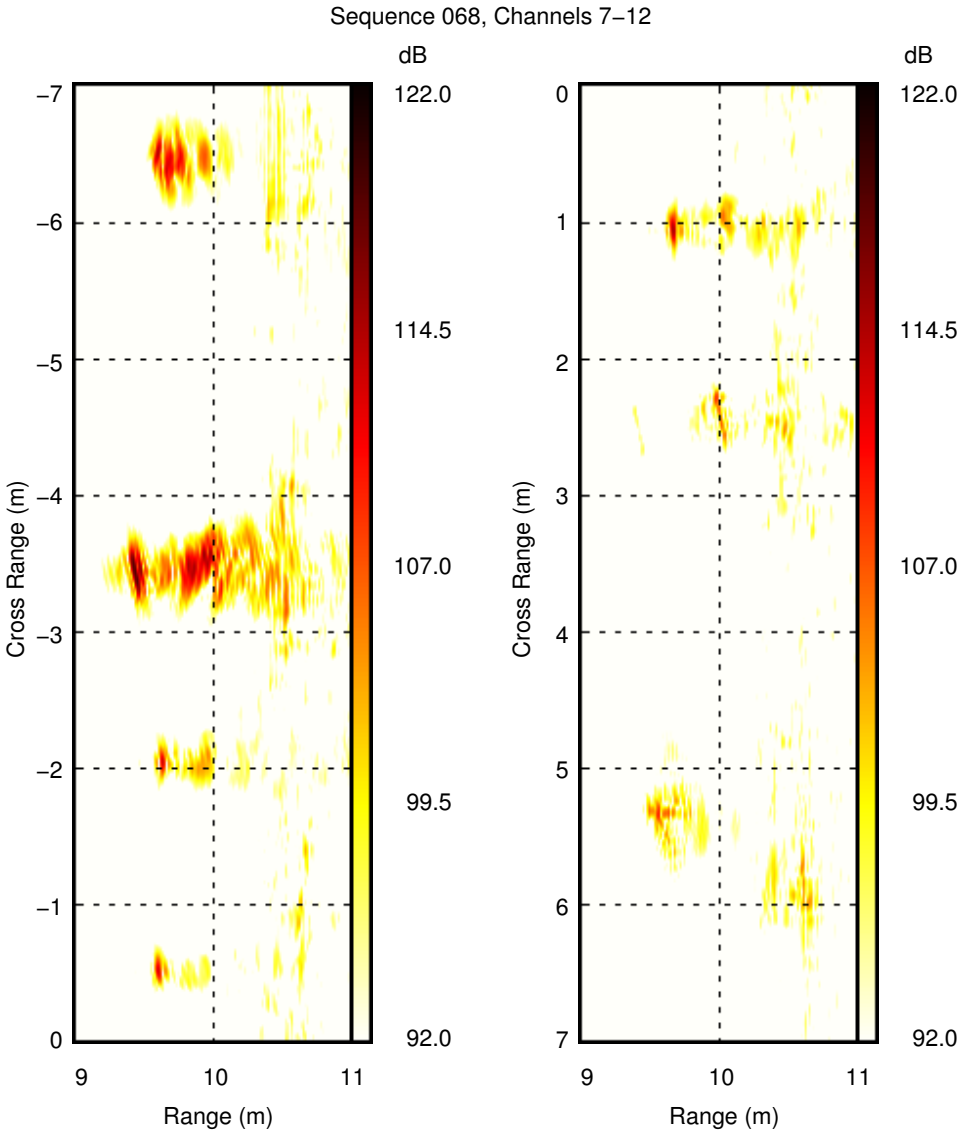

Figure 50: Higher resolution SAS image for sequence 68.

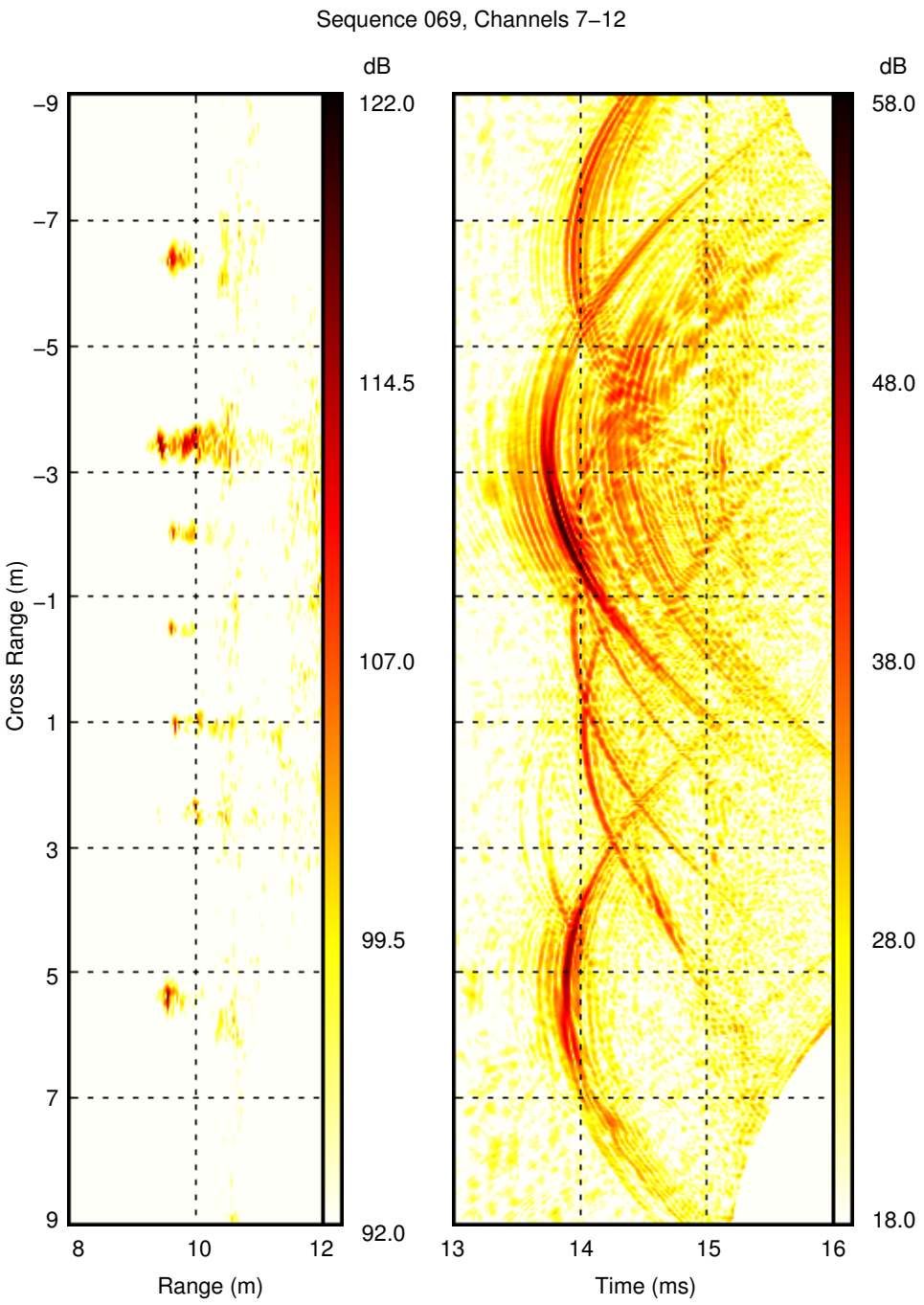

Figure 51: SAS image (left) generated from the pulse-compressed baseband time signals (right) for sequence 69.

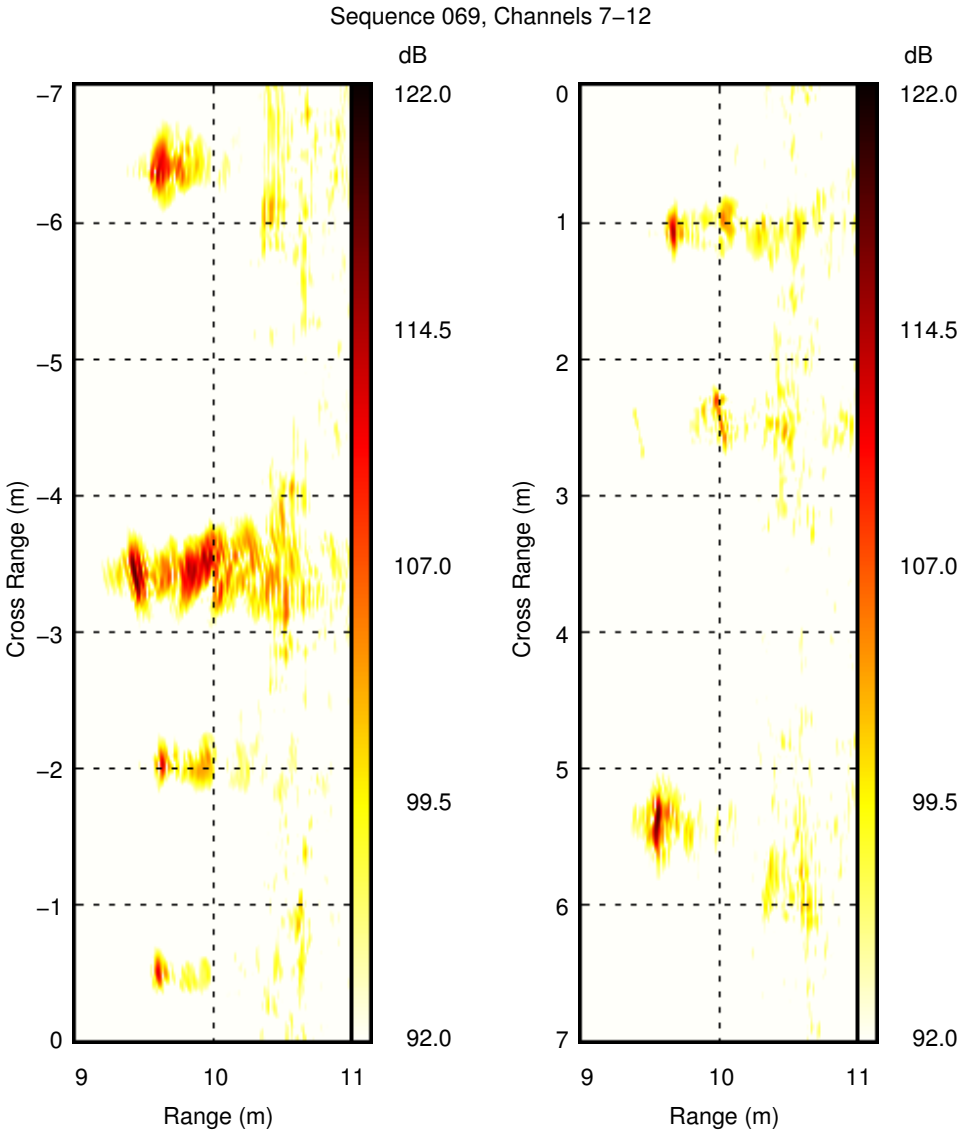

Figure 52: Higher resolution SAS image for sequence 69.